Since January 2020 Elsevier has created a COVID-19 resource centre with free information in English and Mandarin on the novel coronavirus COVID-19. The COVID-19 resource centre is hosted on Elsevier Connect, the company's public news and information website.

Cell Reports

Article

Temporal associations of B and T cell immunity with robust vaccine responsiveness in a 16-week interval BNT162b2 regimen

Graphical abstract

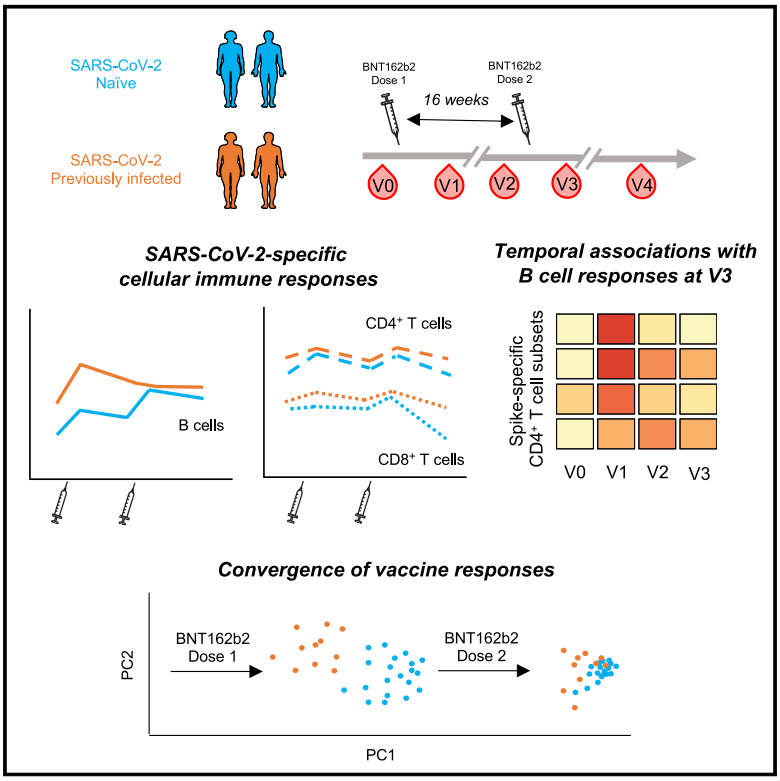

Highlights

- A 16-week interval BNT162b2 regimen generates strong and diverse immune responses
- Features of responses in SARS-CoV-2 naive versus PI donors converge after boost
- The 16-week interval BNT162b2 vaccination leads to development of immune memory
- There are contemporaneous and temporal associations between B and T cell responses

Authors

Manon Nayrac, Mathieu Dubé, Gérémy Sannier, ..., Valérie Martel-Laferrière, Andrés Finzi, Daniel E. Kaufmann

Correspondence

andres.finzi@umontreal.ca (A.F.), daniel.kaufmann@umontreal.ca (D.E.K.)

In brief

Nayrac et al., show that a 16-week interval BNT162b2 regimen elicits robust SARS-CoV-2-specific B and T cell responses in SARS-CoV-2 naive and previously infected individuals. Immune response kinetics differs after the first dose between cohorts but converges after boosting, which elicits a multifaceted cellular recall response and functional memory.

Nayrac et al., 2022, Cell Reports *39*, 111013
June 28, 2022
https://doi.org/10.1016/j.celrep.2022.111013

CellPress

Cell Reports

CellPress
OPEN ACCESS

Article

Temporal associations of B and T cell immunity with robust vaccine responsiveness in a 16-week interval BNT162b2 regimen

Manon Nayrac,[1,2,9] Mathieu Dubé,[1,9] Gérémy Sannier,[1,2,10] Alexandre Nicolas,[1,2,10] Lorie Marchitto,[1,2] Olivier Tastet,[1] Alexandra Tauzin,[1,2] Nathalie Brassard,[1] Raphaël Lima-Barbosa,[3,7] Guillaume Beaudoin-Bussières,[1,2] Dani Vézina,[1] Shang Yu Gong,[1,4] Mehdi Benlarbi,[1] Romain Gasser,[1,2] Annemarie Laumaea,[1,2] Jérémie Prévost,[1,2] Catherine Bourassa,[1] Gabrielle Gendron-Lepage,[1] Halima Medjahed,[1] Guillaume Goyette,[1] Gloria-Gabrielle Ortega-Delgado,[1] Mélanie Laporte,[1] Julia Niessl,[1,2,8] Laurie Gokool,[1] Chantal Morrisseau,[1] Pascale Arlotto,[1] Jonathan Richard,[1,2] Justin Bélair,[3,7] Alexandre Prat,[1,5] Cécile Tremblay,[1,2] Valérie Martel-Laferrière,[1,2] Andrés Finzi,[1,2,4,*] and Daniel E. Kaufmann[1,2,6,11,*]

[1]Centre de Recherche du CHUM, Montréal, QC H2X 0A9, Canada
[2]Département de Microbiologie, Infectiologie et Immunologie, Université de Montréal, Montréal, QC H2X 0A9, Canada
[3]Université de Montréal, Montréal, QC H3T 1J4, Canada
[4]Department of Microbiology and Immunology, McGill University, Montréal, QC H3A 2B4, Canada
[5]Département of Neurosciences, Faculty of Medicine, Université de Montréal, Montréal, QC, Canada
[6]Département de Médecine, Université de Montréal, Montréal, QC H3T 1J4, Canada
[7]Present address: Independent data scientist
[8]Present address: Center for Infectious Medicine, Department of Medicine Huddinge, Karolinska Institutet, Stockholm 171 77, Sweden
[9]These authors contributed equally
[10]These authors contributed equally
[11]Lead contact
*Correspondence: andres.finzi@umontreal.ca (A.F.), daniel.kaufmann@umontreal.ca (D.E.K.)
https://doi.org/10.1016/j.celrep.2022.111013

SUMMARY

Spacing of BNT162b2 mRNA doses beyond 3 weeks raises concerns about vaccine efficacy. We longitudinally analyze B cell, T cell, and humoral responses to two BNT162b2 mRNA doses administered 16 weeks apart in 53 SARS-CoV-2 naive and previously infected donors. This regimen elicits robust RBD-specific B cell responses whose kinetics differs between cohorts, the second dose leading to increased magnitude in naive participants only. While boosting does not increase magnitude of $CD4^+$ T cell responses further compared with the first dose, unsupervised clustering of single-cell features reveals phenotypic and functional shifts over time and between cohorts. Integrated analysis shows longitudinal immune component-specific associations, with early T helper responses post first dose correlating with B cell responses after the second dose, and memory T helper generated between doses correlating with CD8 T cell responses after boosting. Therefore, boosting elicits a robust cellular recall response after the 16-week interval, indicating functional immune memory.

INTRODUCTION

The coronavirus disease 19 (COVID-19) pandemic caused a race for prophylactic vaccines against SARS-CoV-2 (Krammer, 2020), including mRNA-based technologies (Baden et al., 2021; Dickerman et al., 2021; Skowronski and De Serres, 2021; Thomas et al., 2021). These mRNA vaccines target the trimeric Spike glycoprotein that facilitates SARS-CoV-2 entry into host cells via its receptor-binding domain (RBD) (Hoffmann et al., 2020; Walls et al., 2020). Antibody responses are associated with protection for most licensed vaccines and the generation of Spike-specific antibodies, particularly of neutralizing RBD-specific antibodies, is considered critical for SARS-CoV-2 vaccine efficacy. Protective antibody responses are being identified (Earle et al., 2021; Gilbert et al., 2021) but there is a need for a better understanding of B cell memory responses in the context of different vaccine modalities. $CD4^+$ T cell help is critical for development and maintenance of antibody immunity. SARS-CoV-2-specific $CD4^+$ and $CD8^+$ T cells may contribute to recovery from COVID-19 (Bange et al., 2021; Wurm et al., 2020). mRNA vaccines elicit $CD4^+$ T cell responses (Anderson et al., 2020; Lederer et al., 2020; Painter et al., 2021; Prendecki et al., 2021; Rodda et al., 2022; Sahin et al., 2020) that are likely important determinants of vaccine efficacy. $CD4^+$ T subsets include T follicular helper (Tfh) cells that are critical for the expansion, affinity maturation, and memory development of B cells (Crotty, 2019), and T helper 1 (Th1) cells, which foster development of $CD8^+$ T cell memory (Laidlaw et al., 2016). However, T cell

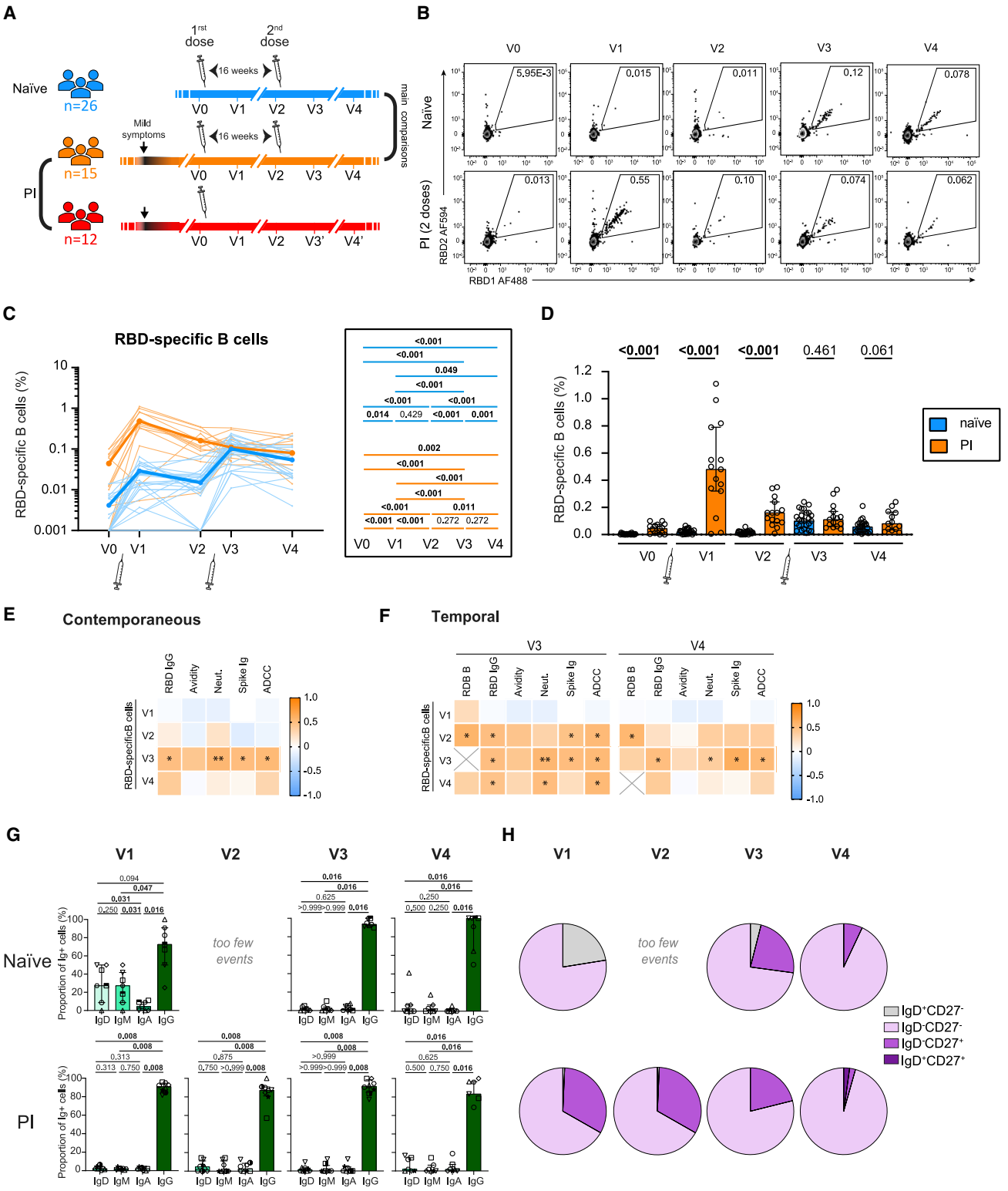

Figure 1. Marked differences in B cell responses to the first BNT162b2 dose between naive and pre-infected participants contrast with convergent features after boosting

(A) Schematic representation of study design. Blood samples were collected at five time points (summarized in Table 1): baseline (V0); 3 weeks (V1) or 12 weeks (V2) after dose 1; 3 weeks (V3) or 16 weeks (V4) after dose 2. For participants receiving a single dose, V3′ was sampled 19 weeks after dose 1 and V4′ 16 weeks after V3′. Dose administrations are indicated by a syringe.

(legend continued on next page)

subsets show important heterogeneity and plasticity, better fitting with spectra of phenotypes and functions than fully distinct populations (O'Shea and Paul, 2010). Unequivocal lineage characterization is therefore challenging, and unsupervised clustering analytical approaches are increasingly used to identify T cell subsets more specifically associated with immunological outcomes (Apostolidis et al., 2021; Maucourant et al., 2020).

The standard BNT162b2 immunization regimen recommends a 21-day interval between vaccine doses, and inoculation of two doses irrespective of prior SARS-CoV-2 infection status. However, the optimal interval has not been determined in controlled trials. In the context of vaccine scarcity and given the significant protection already conferred by the first dose in non-high-risk populations (Baden et al., 2021; Polack et al., 2020; Skowronski and De Serres, 2021), some public health agencies implemented schedules with longer intervals to rapidly extend population coverage (Paltiel et al., 2021; Tuite et al., 2021) and recommended a single dose for previously infected immunocompetent people. Longer delays between doses also frequently occur in real-life settings. While such strategies generated concerns given uncertain immunogenicity, a longer period of partial vulnerability to infection, and a hypothetical risk of escape mutant selection, epidemiological evidence supports this approach as a valid alternative in lower-risk populations (Carazo et al., 2021; Skowronski et al., 2021) in which robust T cell and antibody responses are observed after a single dose (Tauzin et al., 2021b), and stronger and broader antibody immunity induced after the second dose (Grunau et al., 2021; Tauzin et al., 2021a). While significant progress has been made in the understanding of the kinetics of B and T cell responses in short-interval mRNA vaccine schedules (Goel et al., 2021; Painter et al., 2021; Rodda et al., 2022; Zollner et al., 2021), the immunological implications of widely spaced vaccination regimens remain poorly known.

Here, we define the trajectories, differentiation state, and interplay of vaccine-induced Spike-specific B cells, $CD4^+$ T cells, $CD8^+$ T cells, and antibody responses in SARS-CoV-2 naive or previously infected individuals who received two mRNA vaccine doses administered 16 weeks apart, and in a third group of previously infected individuals who received a single vaccine dose.

RESULTS

Study participants

We evaluated immune responses in three cohorts of health care workers (HCW) (Figure 1A): 26 SARS-CoV-2 naive and 15 previously infected (PI) donors who received a two-dose BNT162b2 regimen spaced by 16 weeks; and 12 PI individuals who received a single dose. Blood samples were collected at five time points: at baseline (V0); 3 weeks after the first dose (V1); 12 weeks after the first dose (V2); 3 weeks after the second dose for participants receiving two doses (V3) or 19 weeks after the first dose for the single-dose PI participants (V3′); and 16 weeks after the second dose (V4). Clinical characteristics (Table 1) did not statistically differ between cohorts, except for the numbers of days between V0 and the first dose and for time between the first dose and V2.

Marked differences in B cell responses to the first BNT162b2 dose between naive and PI participants contrast with convergent features after boosting

To evaluate SARS-CoV-2-specific B cells, we focused on RBD to minimize inclusion of B cells cross-reactive to endemic coronaviruses (Hicks et al., 2021; Klumpp-Thomas et al., 2021). Co-detection of two fluorescently labeled recombinant RBD probes greatly enhances specificity (Figure 1B and Anand et al., 2021; flow cytometry panel, Table S1; gating strategy, Figure S1A). We examined the magnitude of RBD-specific B cells (defined as $RBD1^+RBD2^+CD19^+CD20^+$) in the two-dose cohorts (Figures 1C and 1D). In naive individuals, most participants showed no baseline signal. Priming induced significant RBD-specific B cell responses at V1. The second dose elicited a homogeneous brisk recall response at V3 in all participants. Responses subsequently declined at V4 yet remained significantly higher than at pre-boost time points. The pattern markedly differed in PI (Figures 1C and 1D). Consistent with previous SARS-CoV-2 exposure, RBD-specific B cells were already present at V0. This response increased sharply at V1, followed by attrition at V2. We observed no boosting effect after the second dose and no significant decline at V4. The response to the first BNT162b2 dose in PI (V1) differed in magnitude from the second dose in naive (V3) (Figure S1B). Therefore, the RBD-specific B cell kinetics between the two cohorts markedly differed after the first dose, converged after the second dose, and remained close after the subsequent decline observed at V4 (Figure 1D). In single-dose PI, we observed stable B cell responses at V3′ and V4′ compared with V2, comparable with what we observed in two-dose PI, consistent with a steady memory B cell pool after an initial decline between V1 and V2 (Figures S1C and S1D).

We next investigated the relationships between RBD-specific B cell frequencies at the different time points and antibody responses in naive participants: RBD-specific immunoglobulin G (IgG) antibody levels, anti-RBD IgG avidity, neutralization activity, cell-binding ELISA (CBE) antibody levels, and antibody-dependent cellular cytotoxicity (ADCC) (Figures 1E and 1F). RBD-specific B cell responses positively correlated with contemporaneous antibody levels at V3, but not at V1 (Figure 1E). Contemporary correlations were lost at V4. Early V1 B cell

(B) Representative RBD-specific B cell gating.
(C and D) Kinetics of RBD-specific B cell responses in previously naive (blue) or pre-infected (PI; orange) participants receiving two doses. (C) Bold line represents the cohort's median value. Right: statistical comparisons using a linear mixed model. (D) Intercohort comparisons. Bars represent median ± interquartile range. Intercohort statistical comparisons using a linear mixed model are shown.
(E and F) Heatmap showing (E) contemporaneous or (F) temporal correlations of RBD-specific B cells versus the indicated antibody responses (n = 22). Significant correlations by Spearman tests are shown (*$p < 0.05$, **$p < 0.01$).
(G) Frequencies of IgD-, IgM-, IgA-, and IgG-positive cells in RBD-specific memory B cells in naive and PI donors, with Wilcoxon tests. Bars represent median ± interquartile range.
(H) Proportion of $IgD^{+/-}$ and $CD27^{+/-}$ populations in RBD-specific memory B cells in naive and PI donors.
In (G) and (H), V2 for naive participants could not be analyzed because of low number of events. In (C) and (D), n = 26 naive and n = 15 PI; in (E), n = 26 naive; in (G) and (H), n = 7 naive and n = 8 PI.

Table 1. Clinical characteristics of the study participants[a]

	Previously naive cohort	Previously infected (PI) cohort		
	Two doses[b]	Two doses[b]	Single dose[c]	Entire (PI) cohort
BNT162b2 vaccine	(n = 26)	(n = 15)	(n = 12)	(n = 27)
Variable				
Age	51 (41–56)	47 (43–56)	51 (34–62)	48 (39–59)
Sex				
Male	11 (42%)	10 (66%)	4 (33%)	14 (52%)
Female	15 (58%)	5 (34%)	8 (66%)	13 (48%)
Previous SARS-CoV-2 infection				
Days between day of symptom onset and first vaccine dose	NA	274 (258–307)	287 (227–306)	281 (250–307)
Vaccine dose spacing				
Days between doses 1 and 2	111 (109–112)	110 (110–112)	NA	NA
Visits for immunological profiling				
V0, days before first dose	**1 (0–5)**	**24 (6–43)**	**18 (7–45)**	**23 (6–43)**
V1, days after first dose	21 (19–26)	20 (19–21)	20 (18–21)	20 (18–21)
V2, days after first dose	**83 (82–84)**	**89 (86–93)**	**90 (87–94)**	**89 (86–93)**
V2, days before second dose	28 (26–29)	23 (18–28)	NA	NA
V3, days after first dose	133 (130–139)	138 (132–142)	132 (130–138)	136 (131–141)
V3, days after second dose	21 (20–27)	22 (18–28)	NA	NA
V4, days after first dose	224 (222–228)	224 (222–227)	227 (223–237)	NA
V4, days after second dose	112 (110–119)	113 (110–117)	NA	NA

[a]Values displayed are medians, with interquartile range in parentheses for continuous variables or percentages for categorical variables.
[b]The previously naive cohort and previously infected cohort that also received two vaccine doses were compared by the following statistical tests: for continuous variables, Mann-Whitney U test; for categorical variables, Fisher's test. Values in bold are statistically different between the pre-infected naive and pre-infected cohorts. No statistical difference was found between the two pre-infected subcohorts, except between naive and pre-infected for days before V0 and days after V2.
[c]The previously infected cohort with one dose was likewise compared with the previously infected cohort that received two doses. No significant differences were observed between the two cohorts.

responses were not associated with subsequent V3 and V4 antibody responses, but significant correlations were found between RBD-specific B cells at V2 and RBD IgG, total Spike antibody, cell binding, and ADCC at V3 (Figure 1F). Similarly, V3 RBD-specific B cell responses correlated significantly with V4 RBD-specific IgG, total anti-Spike antibody levels, and ADCC, suggesting that the B cell pool post boost conditioned the long-term quantity and quality of the humoral response.

To determine how B cell populations qualitatively evolved, we measured IgD, IgM, IgG, and IgA expression in RBD-specific B cells. In the naive cohort, we detected subpopulations of IgD^+, IgM^+, and IgA^+ cells at V1, whose proportion decreased at V3 and V4 visits. In contrast, RBD-specific memory B cells in PI donors were almost entirely IgG^+ at all time points (Figures 1G, S1E, and S1F). To assess B cell differentiation, we quantified IgD and CD27 co-expression (Figure S1G). CD27 is predominantly expressed on memory B cells (Tangye et al., 1998), and IgD on unswitched B cells (Moore et al., 1981). In the naive cohort, IgD^+CD27^- RBD-specific B cells present at V1 disappeared at V3, while IgD^-CD27^+ RBD-specific B cells emerged (Figure 1H), consistent with isotype-switched memory B cells. This subset contracted at V4. In PI, IgD^-CD27^+ cells already present at baseline expanded after priming and remained stable at V2. Boosting did not further expand this subset. Instead, it gradually declined at V3 and V4. A class-switched IgG^+ DN population dominated at all time points (Figures 1H, S1H, and S1I).

These data show that despite the long 16-week interval and the divergent RBD-specific B cell trajectories after the first dose, boosting in naive subjects induced robust recall responses with a mature phenotype that converged with those observed in PI individuals.

The first and delayed second vaccine doses elicit Spike-specific $CD4^+$ T cell responses of similar magnitude

$CD4^+$ T cells help play a critical role in development of B cell and $CD8^+$ T cell immunity. We measured Spike-specific T cell responses at the V0–V4 time points in the three cohorts (Figures 2 and S2). As in our previous work (Tauzin et al., 2021b), we used a T cell receptor-dependent activation-induced marker (AIM) assay that broadly identifies antigen-specific T cells and functional profiling by intracellular cytokine staining (ICS) (for flow cytometry panels, see Tables S2 and S3).

The AIM assay involved a 15-h incubation of peripheral blood mononuclear cells (PBMCs) with an overlapping peptide pool spanning the Spike coding sequence and the upregulation of CD69, CD40L, 4-1BB, and OX-40 upon stimulation. We used an AND/OR Boolean combination gating to assess total

frequencies of antigen-specific $CD4^+$ and $CD8^+$ T cells (Figures S2A and S2B) (Niessl et al., 2020a). At V3, all individuals had $CD4^+$ T cell responses (Figure S2C), and most had $CD8^+$ T cell responses (Figure S2D).

In contrast to B cell responses, the kinetics of Spike-specific AIM^+CD4^+ T cell responses was similar between naive and PI individuals (Figure 2A). Several naive participants had detectable AIM^+CD4^+ T cell responses at baseline, probably due to cross-reactivity with other coronaviruses (Mateus et al., 2020). The significant increase at V1 was followed by a moderate attrition at the V2 memory time point. The second dose significantly boosted the responses at V3 in naive, whereas the increase was non-significant in PI. No significant differences in median magnitude of AIM^+CD4^+ T cell responses were observed at V1 and V3 between naive and PI, although a faster decay in naive created a significant difference at V4 (Figure 2B).

The ICS assay involved a 6-h stimulation with the Spike peptide pool and measurement of effector molecules interferon-γ (IFN-γ), interleukin-2 (IL-2), tumor necrosis factor α (TNF-α), IL-17A, IL-10, and CD107a. We defined $cytokine^+CD4^+$ T cell responses by an AND/OR Boolean gating strategy (Figure S2E). The ICS patterns in both cohorts paralleled the AIM assays, albeit at a lower magnitude (Figures 2C, 2D, and S2F). Consistent with the lower ability of ICS to detect memory cells compared with recently primed or reactivated cells (da Silva Antunes et al., 2018), the relative increase in $cytokine^+CD4^+$ T cells was stronger at V1 versus V0 and V3 versus V2. $Cytokine^+CD4^+$ T cell responses at V4 remained significantly higher than at baseline, showing longer-term memory, but without significant gain compared with V2.

The magnitude of Spike-specific AIM^+ T cell responses was globally lower in $CD8^+$ than in $CD4^+$ T cells (Figures 2E, 2F, and S2G). The trajectories of AIM^+CD8^+ T responses were heterogeneous. Naive participants elicited weak but significant responses after priming, and a trend for stronger responses after the boost. There was higher heterogeneity in PI, consistent with variable pre-existing responses before vaccination. Several PI showed robust responses after the priming and boosting inoculations, although the increase did not reach statistical significance (Figure 2E). AIM^+CD8^+ T cell responses declined significantly at V4 for naive participants while the decrease was slower for the PI cohort. Total $cytokine^+CD8^+$ T cell responses were weak or undetectable in most participants, precluding their detailed analysis (Figure S2H).

To define the evolution of T cell responses in the absence of boosting, we examined the single-dose PI cohort. In these participants, the magnitude of AIM^+CD4^+ (Figure S2I), AIM^+CD8^+ (Figure S2J), and $cytokine^+CD4^+$ (Figure S2K) T cell responses did not further decline at V3′, suggesting stable early memory. We did not observe significant differences in AIM^+CD4^+ and $CD8^+$ T cell responses between this V3′ time point in the single-dose PI cohort compared with the V3 post boost in the two-dose PI cohort, while we saw stronger $cytokine^+CD4^+$ T cell responses in the two-dose PI cohort. The boost helped maintain higher T cell responses at the V4 late memory time point, with a significant difference for the AIM^+CD4^+ T responses (Figures S2L–S2N).

As expansion of previously primed antigen-specific T cells may impact T cell responses to vaccination, we examined correlations across visits (Figure 2G) and found a significant association or a strong trend between $CD4^+$ T cell responses at V0 and the post-first-dose time points V1 and V2, but not after the second dose. Similar to $CD4^+$ T cells, we observed that pre-existing $CD8^+$ T cell responses at V0 significantly correlated with responses to the first dose at V1, and that this association disappeared after the second dose (Figure 2H). Therefore, the second vaccine dose reduced the heterogeneity in magnitude of T cell responses and its link to pre-vaccination immunity.

These data show that a single dose of the BNT162b2 is sufficient to induce CD4 Th and $CD8^+$ T cell responses in most participants. After a 16-week interval, the second dose boosts $CD4^+$ and $CD8^+$ T cell responses back to the peak magnitudes reached soon after priming. Pre-vaccination T cell immunity is associated with the BNT162b2-induced $CD4^+$ and $CD8^+$ T cell responses to the first vaccination, but this correlation is lost after boosting.

The 16-week interval BNT162b2 regimen elicits phenotypically diverse $CD4^+$ T helper subsets

We next profiled the qualitative heterogeneity and evolution of Spike-specific AIM^+CD4^+ T cells. To avoid a priori defined marker combinations, we performed unsupervised analyses of the high-dimensional flow cytometric phenotyping data (Figure 3). We examined chemokine receptors that are preferentially, but not exclusively, expressed by some lineages and involved in tissue homing (CXCR5 for Tfh; CXCR3 for Th1; CCR6 for Th17/Th22 and mucosal homing; CXCR6 for pulmonary mucosal homing [Day et al., 2009; Morgan et al., 2015]), CD38 and HLA-DR as activation markers, and PD-1 as inhibitory checkpoint.

We illustrated the distribution of clustered populations by the uniform manifold approximation and projection (UMAP) algorithm (Becht et al., 2018). Cluster identity was performed using Phenograph (Levine et al., 2015), resulting in the identification of ten clusters (Figures 3A and 3B) based on distinct profiles of relative marker expression (Figures 3C and S3A). All ten clusters were detectable at V0 and persisted at all time points. The relative frequencies of each cluster did not show major differences across visits (Figure 3D), but there were fluctuations and interindividual variations within cohorts (Figures 3E and S3B). We did not observe emergence of new Th clusters after the second inoculation. While variability and relatively small cohort size precluded definitive conclusions about the behavior of individual clusters, some general trends were observed. In naive, most clusters showed either a significant increase or a trend for increase after the second dose (Figure 3E), except C4 (Figure S3B). These included clusters enriched in CXCR5 (C3 and C5) and CXCR3 (C2, C3, and C10). In contrast, the qualitative response to the second in PI was more constrained (Figures 3D and S4C). Consistent with the analysis of total AIM^+CD4^+ cells, all naive participant clusters declined at V4, except C4 (Figures 3E and S3B). Although some clusters also showed a trend for decline in PI (C5, C6, C9, and C10), most did not (C1, C2, C3, C4, C7, and C8).

We next performed univariate analyses of chemokine receptor expression (Figures 3F–3K and S3D–S3I). $CXCR5^+AIM^+CD4^+$ T cells increased after both doses in naive individuals, but only after the first dose in PI (Figure 3F). Trajectories did not

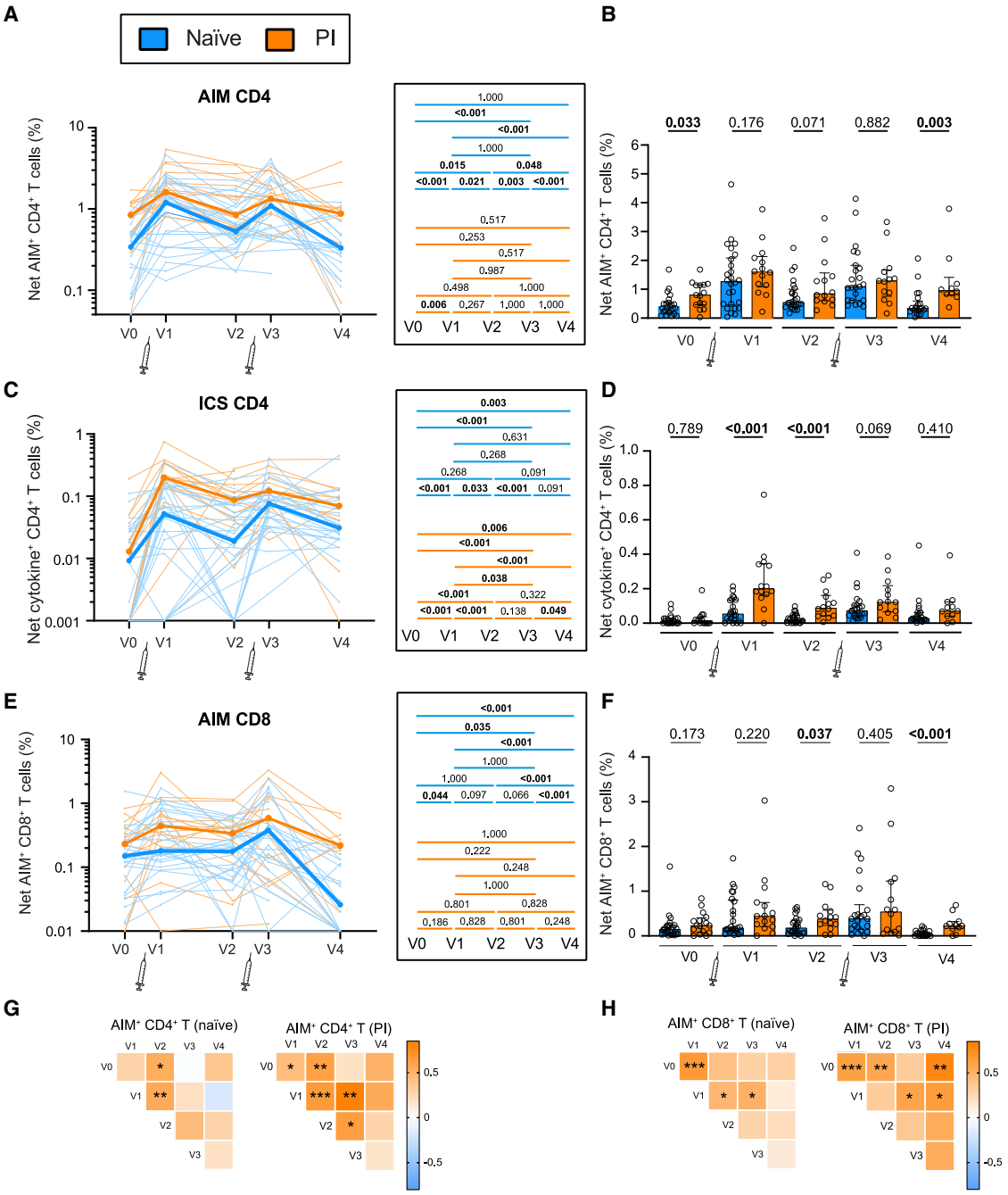

Figure 2. The first and delayed second vaccine doses elicit Spike-specific CD4⁺ T cell responses of similar magnitude

SARS-CoV-2 Spike-specific CD4⁺ and CD8⁺ T cells in naive (blue) and PI (orange) receiving two vaccine doses.

(A–F) (A and B) Longitudinal (A) and intercohort (B) analyses of net Spike-specific AIM⁺CD4⁺ T cell responses. Right: statistical comparisons. (C and D) Longitudinal (C) and intercohort (D) analyses of the net magnitude of cytokine⁺CD4⁺ T cell responses. (E and F) Longitudinal (E) and intercohort (F) analyses net AIM⁺CD8⁺ T cell responses. The bold lines in (A), (C), and (E) represent median values. The bars in (B), (D), and (F) represent median ± interquartile range. In (A), (C), and (E), the syringe indicates vaccine dose inoculation and the right-hand panels show statistical comparisons. Pairwise (A, C, E) and intercohort (B, D, F) statistical analyses were performed using a linear mixed model.

(G and H) Heatmap showing temporal correlations of (G) AIM⁺CD4⁺ and (H) AIM⁺CD8⁺ T cells between the different time points for naive and PI participants. Significant Spearman test results are indicated (*p < 0.05, **p < 0.01, ***p < 0.001).

In (A) to (F), n = 26 naive and n = 15 PI; in (G) and (H), n = 26 naive and n = 27 PI (comparisons at time points V0, V1, and V2), and n = 15 PI (comparisons at time points V3 and V4).

CellPress
OPEN ACCESS

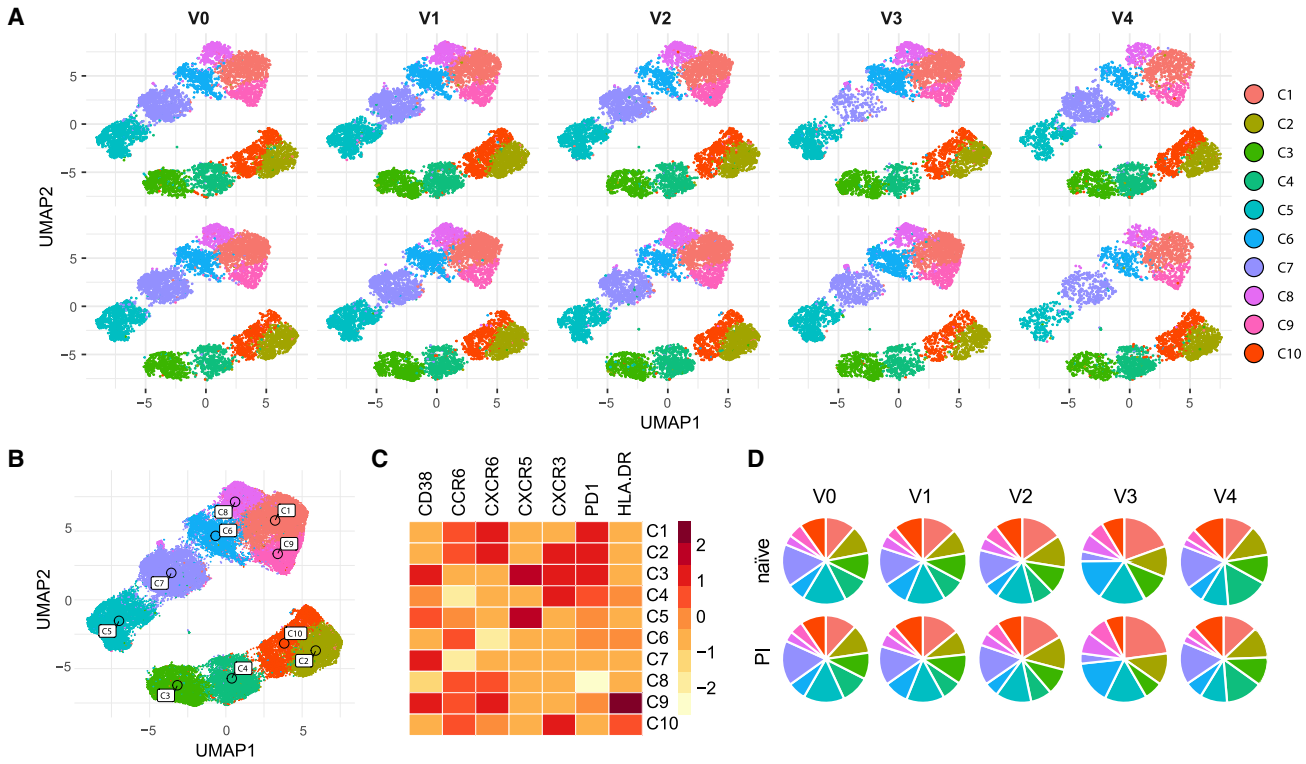

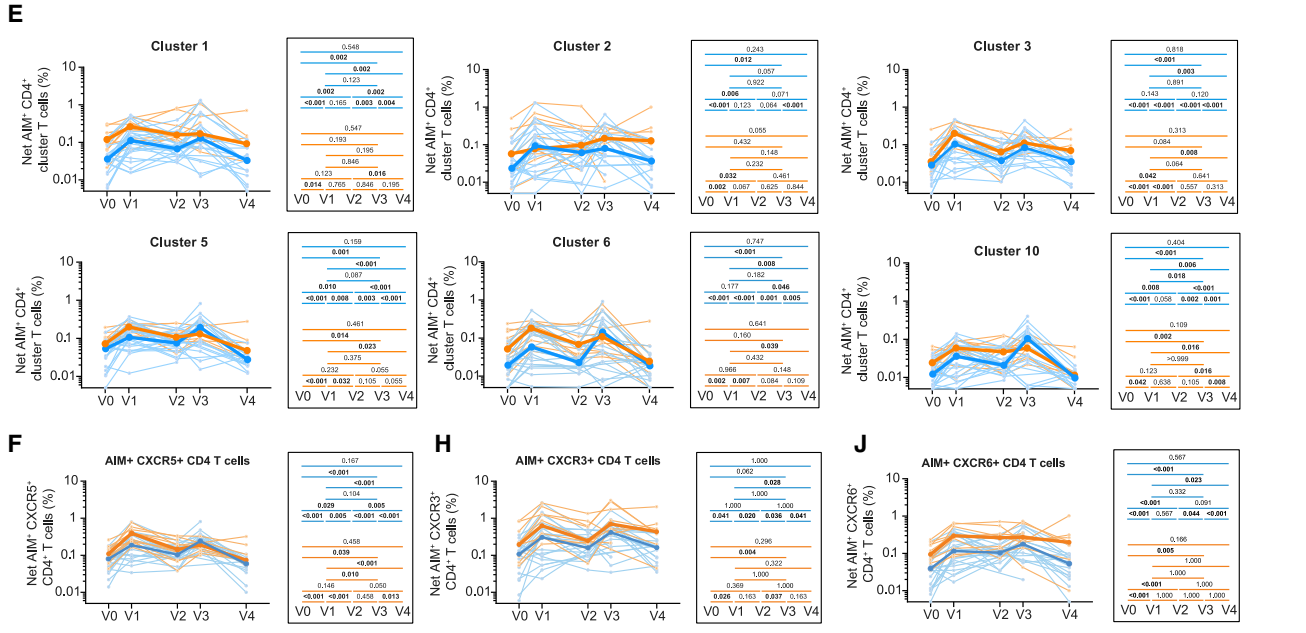

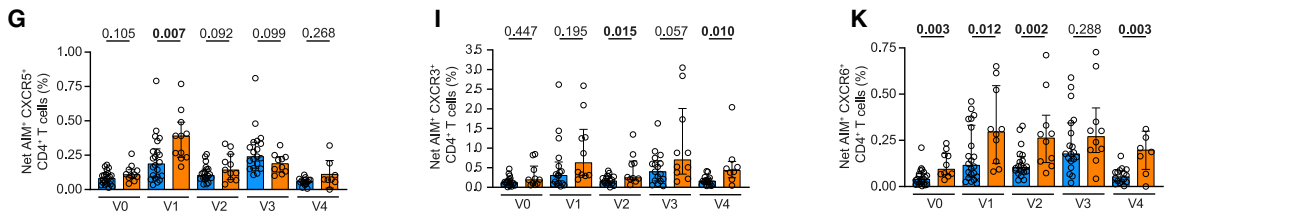

(legend on next page)

statistically differ between cohorts past V1 (Figure 3G). $CXCR3^+AIM^+CD4^+$ T cells increased similarly after either dose, with significant decline post first inoculation (Figure 3H). This pattern was similar in naive and PI, but the $CXCR3^+$ subset was more abundant in PI (Figure 3I). $CXCR6^+AIM^+$ (Figures 3J and 3K) and $CCR6^+AIM^+CD4^+$ T cells (Figures S3H an S3I) remained persistently elevated after priming in PI, while in naive they were weaker at early time points but responsive to the second dose at V3. However, they declined at the late memory time point V4 in this cohort.

Therefore, the first vaccine dose already elicits phenotypically diverse Th clusters that do not necessarily fit with canonical lineages. The second vaccine dose variably impacted these subsets but did not elicit new clusters. Th phenotype in PI was enriched in markers, suggestive of prior mucosal priming.

The delayed second BNT162b2 dose leads to partially convergent functional profiles in naive and PI participants

We next applied the same unsupervised analysis pipeline to Spike-specific $cytokine^+CD4^+$ T cells for the six functions measured, identifying 11 clusters (Figures 4A–4C and S4A) that were present at all time points (Figures 4A and 4D), with notable interindividual differences within each cohort (Figures 4E and S4B). However, we observed clearer functional differences between cohorts and between doses when compared with phenotypic analysis. Most clusters increased after both doses in naive, whereas they expanded only after the first dose in PI (Figures 4E and S4B). Individual clusters followed different trajectories depending on pre-infection status (Figures 4E and S4C). The evolution of the IL-2 enriched C1, the most abundant cluster, was similar in the PI and naive cohorts, except for significant contraction at V4 in naive only. In contrast, the C2 and C3 clusters, characterized by high IFN-γ expression, were markedly larger in PI after the first dose, but responded more to the second dose in naive. Consequently, the responses of C2 and C3 partially converged at V3 compared with V1; they significantly contracted at V4. The polyfunctional cluster C5, enriched in IFN-γ, IL-2, TNF-α, and CD107a, showed yet another pattern: it was expanded in PI compared with naive at all time points, and showed excellent long-term stability in both cohorts.

Single-parameter analyses (Figures 4F–4K) showed that in naive participants the first dose significantly increased IFN-γ^+ and IL-2^+ $CD4^+$ T cell responses, with a strong trend for an increase in TNF-α^+ responses. The increase in ICS responses was greater in PI. The second dose significantly boosted these responses in naive only, contrasting with little effect in PI. These differential trajectories led to partially convergent $CD4^+$ T cell functions after repeated antigenic challenges in naive and PI at V3. However, consistent with AIM measurements, weaker responses in naive at V4 led to re-emergence of significant differences at this late memory time point.

These analyses show that pre-infection status is associated with significant differences in the functional profile elicited by the first BNT162b2 dose. Preferential expansion of Th1-cytokine-enriched subsets after boosting in naive participants contrasting with stable responses in PI leads to partial, and possibly transient, convergence of Th functions between cohorts after full vaccination. The unsupervised analysis reveals a polyfunctional cluster of $CD4^+$ T cells stably maintained at the late memory time point.

Temporal relationships between antigen-specific $CD4^+$ T cell, B cell, and $CD8^+$ T cell responses

As $CD4^+$ T cell help is essential for optimal adaptive B cell and $CD8^+$ T cell immunity, we next examined the temporal associations between these immune components (Figure 5). We considered the total Spike-specific AIM^+CD4^+ T cells, the AIM^+C1-C10 clusters, the total Spike-specific $cytokine^+CD4^+$ T cells, and the ICS ($cyto^+$C1–C11) clusters at time points V0–V3. We applied unsupervised clustering analyses to determine the longitudinal relationships between these Th subsets and RBD-specific B cell (Figure 5A) and AIM^+CD8 T cell (Figure 5B) responses, measured at V3 after completing the vaccination regimen.

We observed significant positive correlations between all AIM^+CD4^+ T cell subsets elicited at V1 and the B cell responses at V3 after the second dose (Figure 5A). This contrasted with the weaker correlations between V2–V3 $cytokine^+$ Th responses and RBD-specific B cells at V3. Some of the positively correlated clusters (AIM^+C3, AIM^+C5) were enriched in $CXCR5^+$ cells. Consistently, $CXCR5^+AIM^+CD4^+$ T cell responses at V1 strongly correlated with B cell responses at V3, but this association weakened for V2 and disappeared at V3 (Figure 5C). Similar patterns were seen with total AIM^+CD4^+ T cells (Figure S5A) and for some non-circulating Tfh (cTfh) subsets, but we did not have the statistical power to rank the strength of the correlations.

We next examined the temporal associations between longitudinal Th subsets and AIM^+CD8^+ T cells at V3 (Figure 5B). Th responses at V1 showed no significant correlation with AIM^+CD8^+ T cells at V3. However, we found significant correlations between $cytokine^+CD4^+$ T cell subsets at the pre-boost V2 memory time point or at the contemporaneous V3 and the AIM^+CD8^+ T cell responses at V3, and IFN-γ^+CD4^+ T cells at V2 correlated with AIM^+CD8^+ T cells at V3 (Figure 5D), as did total $cytokine^+CD4^+$ T cell responses (Figure S5B).

Figure 3. The 16-week interval BNT162b2 regimen elicits phenotypically diverse $CD4^+$ T helper subsets

(A) Multiparametric UMAP representation of Spike-specific AIM^+CD4^+ T cells at each time point, with aggregated data for the two-dose naive and PI cohorts. The colors identify ten populations clustered by unsupervised analysis.

(B) Clusters are labeled on the global UMAP.

(C) Heatmap summarizing mean fluorescence intensity of each loaded parameter.

(D) Pie charts depicting the proportion of each identified cluster within total AIM^+CD4^+ T cells.

(E, F, H, and J) Longitudinal frequencies of selected AIM^+CD4^+ T cell (E) clusters and (F) CXCR5-expressing, (G) CXCR6-expressing, and (H) CXCR3-expressing AIM^+CD4^+ T cells. Bold lines represent cohort's median value. Right: Wilcoxon tests for each pairwise comparison.

(G, I, and K) Cohort comparisons at each time point for (G) CXCR5-expressing, (I) CXCR3-expressing, and (K) CXCR6-expressing AIM^+CD4^+ T cells. Bars represent median ± interquartile range.

In (A) to (K), n = 22 naive and n = 11 PI.

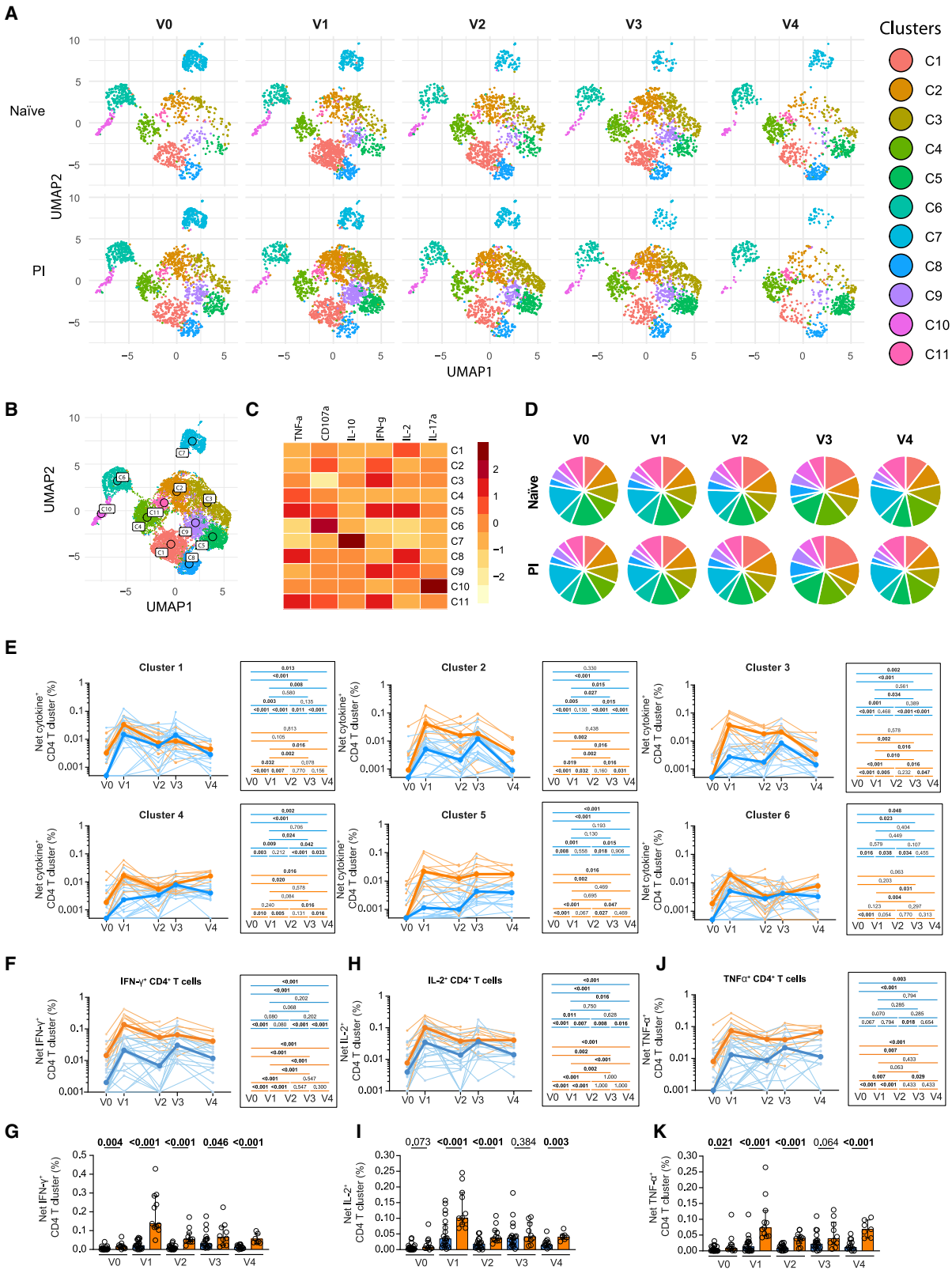

(legend on next page)

The differential temporal associations between antigen-specific CD4$^+$ T cell, B cell, and CD8$^+$ T cell immunity suggest different requirements for the coordination of these responses.

Immune profile kinetics in naive and PI vaccinees shows only partial, and transient, convergence after the delayed second dose

Our data suggest that the relationships between the different immune parameters after the first vaccine dose were strongly influenced by prior infection history, while its impact decreased, but did not disappear, after the second dose. We performed an integrated analysis of 34 features of antibody, B cell CD4$^+$ T cell, and CD8$^+$ T cell responses (Figure 6A). V1–V4 time points were first loaded altogether (Figure 6B), then from this master principal component analysis (PCA) we depicted each time point separately (Figure 6C). The two cohorts clustered apart at V1 due to a significant difference in principal component 1 (PC1) (Figure 6D). The distance between groups decreased upon attrition of the responses (V2). No statistical difference between naive and PI PC1 was observed at V3, showing convergence of the immune features. Importantly, however, the PC1-driven distinction between naive and PI re-emerged at the late memory time point V4.

We sought to identify the features underlying the group clustering at V1 using the same approach focused on AIM$^+$CD4$^+$ and cytokine$^+$CD4$^+$ T cell responses. The correlation between the immune features and PC1 identified anti-RBD IgG levels, memory RBD-specific B cells, and IFN-γ-enriched Spike-specific CD4$^+$ T cell clusters with little contribution of AIM$^+$CD4 T cells. A PCA analysis performed using AIM$^+$CD4$^+$ T cell features confirmed the limited contribution of these features to cohort clustering (Figure S6A), in contrast to the cytokine$^+$CD4$^+$ T cells (Figure S6B).

Therefore, unsupervised integrated analysis shows that pre-infection status shapes a vaccine-induced hybrid immunity after the first dose, while its influence largely wanes in the short-term response to the second dose but subsequently becomes more manifest again 8 months after initial inoculation.

DISCUSSION

The decision to extend intervals between doses of the BNT162b2 mRNA vaccine led to concerns about vaccine immunogenicity and efficacy. Here, we profiled the B cell, CD4$^+$ T cell, CD8$^+$ T cell, and antibody responses in SARS-CoV-2 naive and PI individuals who received the two vaccine doses 16 weeks apart. We longitudinally followed these immune features from baseline over an 8-month period to determine the characteristics and temporal associations of the immune features elicited by this wide-interval immunization regimen.

We observed that in naive participants, the priming dose elicited RBD-specific responses of low magnitude, a strong increase after the second dose administered after 16 weeks, and a moderate contraction in the following months. These robust B cell responses were associated with the development of strong and broad humoral responses, as we reported (Tauzin et al., 2021a). The phenotypic changes were consistent with B cell maturation. However, while we observed the expansion of a CD27$^+$IgD$^-$ memory subset after the second dose compared with the first dose, a majority of double-negative (CD27$^-$IgD$^-$) cells was measured at all time points. This phenotypic subset was described in autoimmune diseases (Jenks et al., 2018; Wei et al., 2007) and in response to vaccination (Ruschil et al., 2020). Their transcriptional program is distinct from canonical switched memory cells and naive cells (Jenks et al., 2018). They may be associated with an extrafollicular maturation pathway (Ruschil et al., 2020). In our study, the long-lasting persistence of these cells and their expression of RBD-specific IgG may suggest an atypical switched memory subset. These data are consistent with development of functional memory B cells with robust recall potential, alleviate the concern that an extended-interval regimen would lead to poor antibody immunity, and are in line with recent findings (Parry et al., 2021; Payne et al., 2021).

The kinetics of B cell responses differed in PI and naive individuals: the first vaccine dose elicited a brisk expansion of RBD-specific B cells in PI, with subsequent partial attrition before the delayed boost that did not expand them further. Consequently, B cell responses were similar in naive and PI participants post boost. The responses observed after the first dose are consistent with results from other studies (Efrati et al., 2021; Stamatatos et al., 2021; Tauzin et al., 2021b; Urbanowicz et al., 2021). A previous short-interval regimen study showed a profound impact of the second dose on antigen-specific B cell responses in naive participants, but a limited one in PI, with convergent trajectories between the groups (Goel et al., 2021). Our results demonstrate that this holds true after an extended 16-week interval, consistent with the limited quantitative and qualitative enhancement of humoral immunity we previously reported (Tauzin et al., 2021a). It further suggests that pre-infection can accelerate the generation of stable memory RBD-specific B cell responses.

CD4$^+$ T cell responses were already quantitatively robust after the first dose. Although variable in magnitude, they were induced

Figure 4. The delayed second BNT162b2 dose leads to partially convergent functional profiles in naive and PI participants

(A) Multiparametric UMAP representation of Spike-specific ICS cytokine$^+$CD4$^+$ T cells at each time point, with aggregated data for the two-dose naive and PI cohorts. The colors identify 11 populations clustered by unsupervised analysis.

(B) Each cluster is labeled on the global UMAP.

(C) Heatmap summarizing the mean fluorescence intensity of each loaded parameter.

(D) Pie charts depicting the proportion of each cluster within total cytokine$^+$CD4$^+$ T cells.

(E, F, H, and J) Longitudinal frequencies of selected cytokine$^+$CD4$^+$ T cell (E) clusters and (F) IFN-γ^+, (H) IL-2$^+$, and (J) TNF-α^+ single functions in naive (blue) and PI (orange) participants. Bold lines represent the cohort's median value. Right: Wilcoxon tests for each pairwise comparison.

(G, I, and K) Cohort comparisons at each time point for (G) IFN-γ^+, (I) IL-2$^+$, and (K) TNF-α^+ single functions. Bars represent median ± interquartile range.

In (A) to (K), n = 22 naive and n = 11 PI.

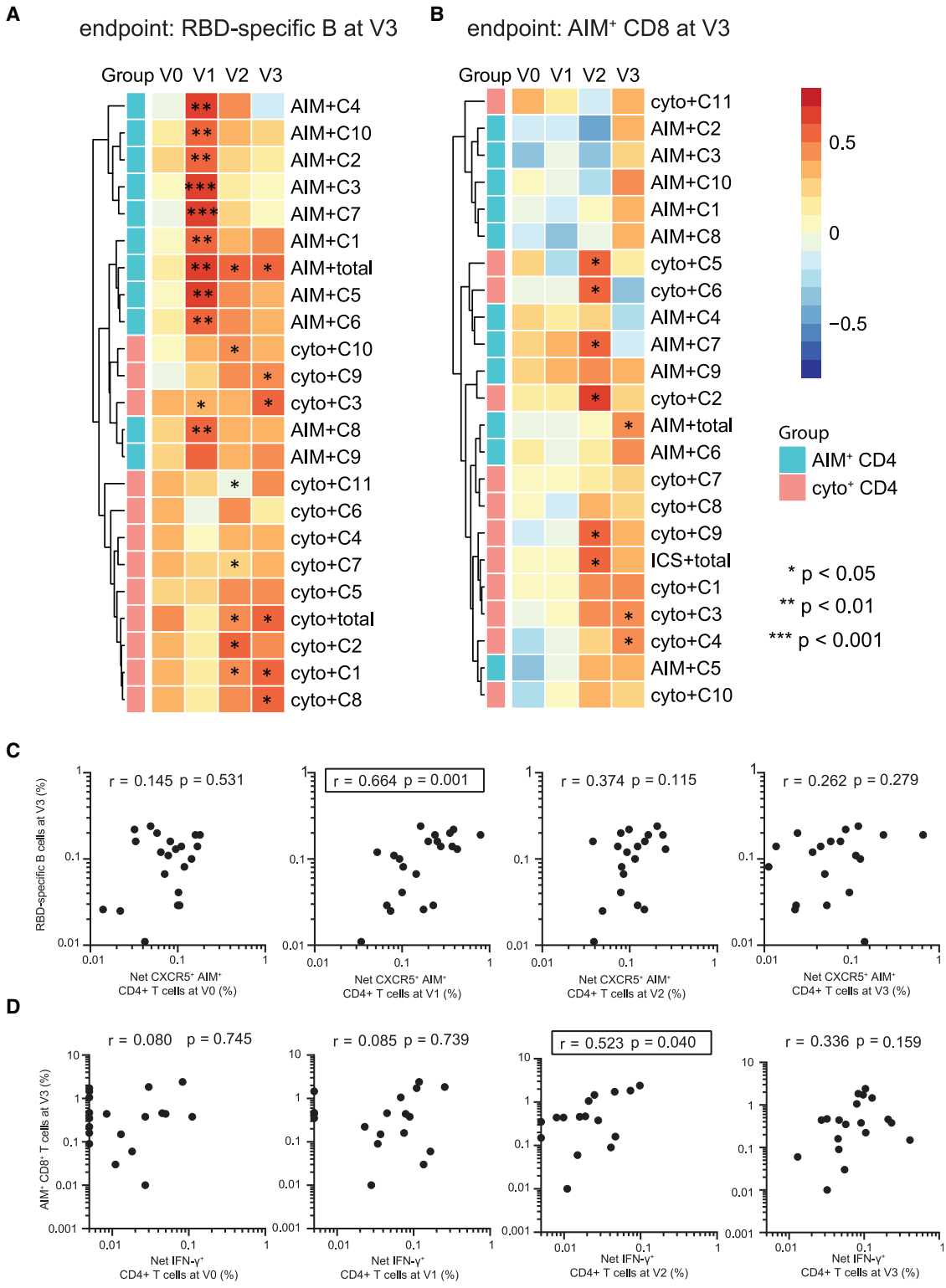

Figure 5. Temporal relationships between antigen-specific CD4+ T cell, B cell, and CD8+ T cell responses in naive participants

(A and B) Heatmaps displaying temporal correlations between the different subsets of Spike-specific CD4+ T cells measured by AIM or ICS assays at the V0, V1, V2, and V3 time points and: (A) RBD-specific B cell frequencies measured at V3; (B) AIM+CD8+ T cell frequencies measured at V3. Asterisks indicate significance (*p < 0.05, **p < 0.01, ***p < 0.001). The CD4+ T cell clusters were stratified by assay (cyan, AIM; light red, ICS).

(legend continued on next page)

in all individuals examined. Mirroring the B cell findings, $CD4^+$ T cell responses decreased moderately before boosting, a contraction to memory that does not have the time to occur in the standard 3-week interval schedule. The second dose reinvigorated Spike-specific $CD4^+$ T responses without surpassing those elicited by the first dose. These trajectories are consistent with short-interval studies (Oberhardt et al., 2021; Painter et al., 2021).

Our unsupervised and supervised analyses demonstrated that the BNT162b2 vaccine elicits a highly diversified $CD4^+$ T cell response, which is maintained over time with no novel distinct subset after the boost. This is consistent with a recent short-delay vaccination study (Rodda et al., 2022). Some qualitative Th features differed between the naive and PI cohorts, and evolved between time points within cohorts. We observed higher frequencies of CXCR6 Th cells in PI than in naive. As CXCR6, the CXCL16 ligand, is a homing molecule to the respiratory mucosa (Day et al., 2009; Morgan et al., 2015), these results are consistent with prior priming of $CD4^+$ T cells at this anatomic site during SARS-CoV-2 infection in PI participants, resulting in differences in their differentiation program, compared with intramuscular vaccine injection. We observed a similar pattern for CCR6, a marker of Th17 and Th22 cells that play an important role in maintaining mucosal barriers and contribute to pathogen clearance at mucosal surfaces (Aujla et al., 2008; Khader et al., 2007). Functional $CD4^+$ T cell subsets also presented differential kinetics between naive and PI individuals but in both cohorts, we identified a polyfunctional Th1 cell subset with excellent temporal stability. An analogous population has been associated with vaccine protection in a murine *Leishmania* model (Darrah et al., 2007). Previous studies reported robust Th1 and Tfh responses after short-delay vaccinations (Goel et al., 2021; Oberhardt et al., 2021; Painter et al., 2021; Sahin et al., 2020). Our unsupervised analyses are consistent with these findings, as such responses defined the bulk of our Spike-specific clusters. Recent unsupervised analyses conducted in short-delay vaccination samples reported that hybrid immunization combining natural and vaccinal challenges imprints partially distinct functional features on SARS-CoV-2-specific $CD4^+$ T cells (Rodda et al., 2022). These imprints attenuated after a third dose. Our data globally suggest that evolution over time contributes to partial convergence between vaccinal and hybrid immunities. Some hybrid immunity imprints were maintained, as we detected a higher frequency of IFN-γ- and TNF-α-rich clusters in PI compared with naive participants at late memory time points.

The hybrid immunity elicited in PI was associated with a more durable immune memory up to 8 months after the first dose. The pattern was particularly pronounced for AIM^+CD8^+ T cells. Besides loss of cytotoxic T lymphocyte (CTL) responses, there are other possible explanations: the measurements in peripheral blood may not reflect persistent tissue-resident memory populations in other anatomic compartments; and the activation-induced markers used may be insensitive to identifying some antigen-specific T cell subsets.

We identified strong temporal associations between several subsets of early vaccine-induced cTfh, a lineage critical for B cell help, and other $CD4^+$ T cell subsets with B cell responses measured several months after the boost, but these correlations were lost at later time points. While the observed disconnect in peripheral blood measurements at the late time points might be related to compartmentalization in lymphoid tissues (rather than major changes in CD4-B cell interplay), they suggest that the early antigen-specific $CD4^+$ T cell responses critically shape the B cell pool, which will later respond to the delayed boosting. Despite the difference in dosing intervals, these results are thus consistent with the immune dynamics observed in the standard regimen (Oberhardt et al., 2021; Painter et al., 2021; Rodda et al., 2022). In contrast, Th1 features identified at the early memory time point were better associated with the CTL responses after full vaccination, and we noted contemporaneous correlations as well. While this might suggest that the responsiveness of $CD8^+$ T cells to boosting benefit from the pre-existing memory Th pool, mechanistic studies in murine models have shown that $CD4^+$ T cell help is key at the time of CTL priming (Laidlaw et al., 2016), although they still play important roles later (Nakanishi et al., 2009). Our observational study does not allow us to delineate causation due to other factors.

While the initial rationale of delaying the second dose was to provide some level of immunity more rapidly to a larger number of people in the context of limiting vaccine supply, our results suggest that this strategy provides strong, multifaceted B and T cell immunity. The potential immunological benefits of increasing the interval between doses must be weighed against a prolonged period of good but still suboptimal protection, particularly while the virus and its different variants of concern are still circulating in the population at epidemic levels. Many countries now recommend a third dose, usually at least 6 months after the second dose. The benefit of a third dose in the context of a 16-week interval between the first and second dose will warrant further investigation.

Limitations of the study

Many individuals in the naive cohort had detectable AIM^+ and $cytokine^+$ T cell responses at baseline. We interpreted this as likely reflecting the presence of a pre-existing pool of cross-reactive cells to other coronaviruses (Grifoni et al., 2020; Shrock et al., 2020; Mateus et al., 2020; Loyal et al., 2021). Formal demonstration in our cohort would require epitope-specific mapping of T cell responses, for which we did not have enough PBMC samples available.

Whether the long interval between doses and/or the pre-infection status affects the differentiation of T cell responses, particularly of vaccine-induced $CD8^+$ T cells, is a question that may impact the efficacy of these responses. We did not address this issue, which will require further studies.

(C) Correlations between frequencies of AIM^+CXCR5^+ $CD4^+$ T cells (for cTfh) at the V0–V3 visits and RBD-specific B cell frequencies at V3.
(D) Correlations between frequencies of IFN-γ^+ (as Th1 function) at the V0–V3 visits and AIM^+CD8^+ T cell at V3. The r and p values from a Spearman test are indicated in each graph.
In (A) and (C), n = 21 naive; in (B) and (D), n = 19 naive.

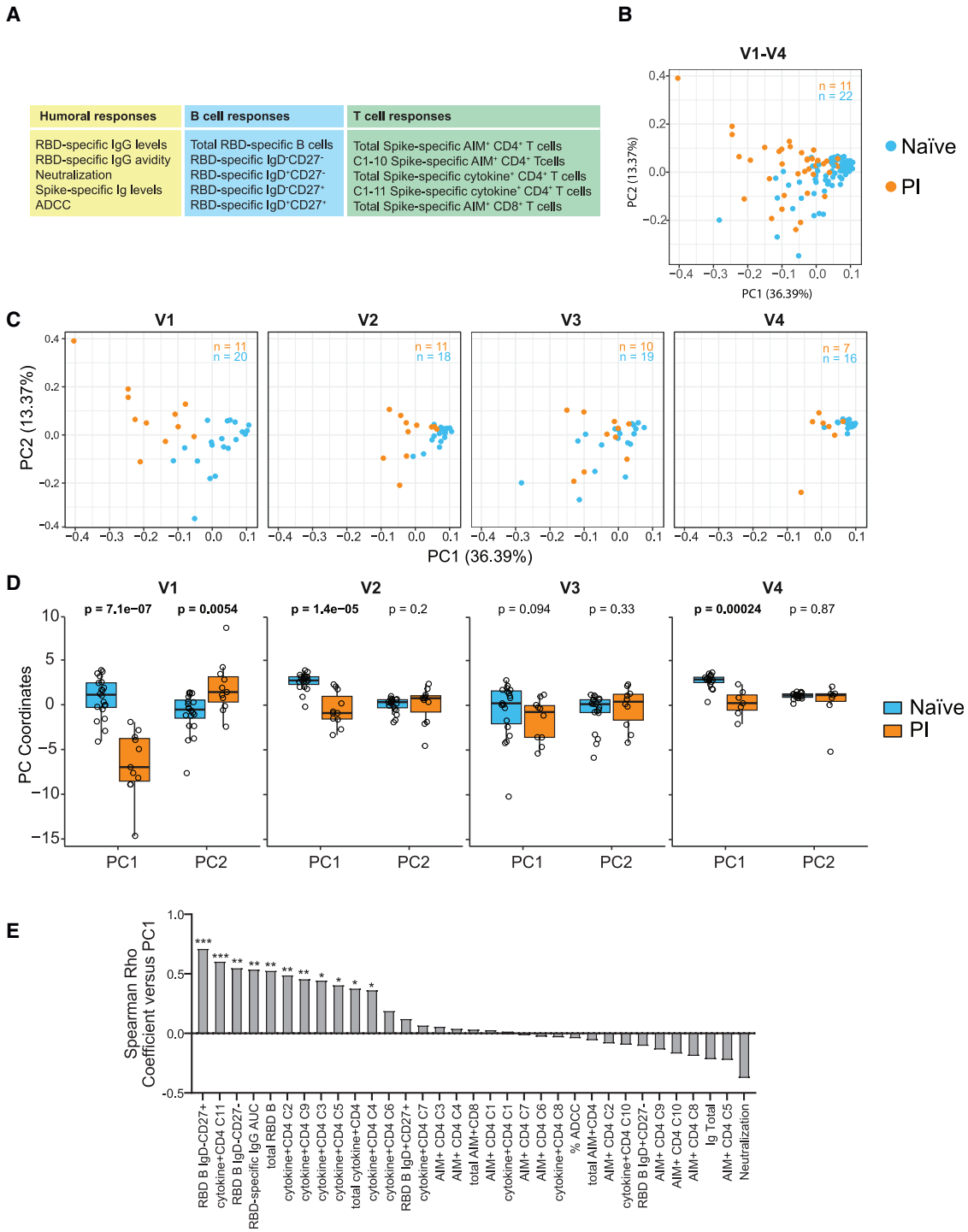

Figure 6. Immune profile kinetics between naive and PI vaccinees shows only partial, and transient, convergence after the delayed second dose

Integrated PCA analysis combining various immune features to compare evolution of vaccine responses in the two-dose naive and PI cohorts.

(A) List of the 34 antigen-specific immune magnitudes included in the PCA analysis.

(B) Global PCA analysis. The percentage on the x and y axes presents the variance attributed to PC1 and PC2, respectively.

(legend continued on next page)

The goal of our study was to provide an in-depth characterization of SARS-CoV-2 vaccine responses. The size of the cohorts investigated here, particularly of the one-dose and two-dose PI cohorts, is not sufficient to robustly prove the benefit of hybrid immunity. However, this question has also been addressed in other reports, with results consistent with our study (Goel et al., 2021; Painter et al., 2021; Rodda et al., 2022).

We did not provide a direct side-by-side comparison of cellular immunity in the long- versus short-interval vaccine regimens. However, in another study, we investigated the impact of dose spacing on antibody responses and demonstrated that the delayed boosting facilitates antibody maturation, resulting in enhanced recognition breadth and neutralization against SARS-CoV-2 variants (Chatterjee et al., 2022).

Our study conducted in a low-risk HCW cohort may not be generalizable to vulnerable groups, particularly immunocompromised or elderly populations, in which the immune responses and the risk/benefit ratio may differ. Future studies will be required to better quantify the immune response over time in these populations.

STAR★METHODS

Detailed methods are provided in the online version of this paper and include the following:

- KEY RESOURCES TABLE
- RESOURCE AVAILABILITY
  - Lead contact
  - Materials availability
  - Data and code availability
- EXPERIMENTAL MODEL AND SUBJECT DETAILS
  - Ethics statement
  - Participants
  - PBMCs and plasma collection
  - Cell lines
- METHOD DETAILS
  - Protein expression and purification
  - RBD-specific IgG levels and avidity measured by enzyme-linked immunosorbent assay (ELISA)
  - Spike IgG levels measured by cell-based ELISA (CBE)
  - ADCC assay
  - Virus neutralization assay
  - SARS-CoV-2-specific B cells characterization
  - Activation-induced marker (AIM) assay
  - Intracellular cytokine staining (ICS)
- QUANTIFICATION AND STATISTICAL ANALYSIS
  - Statistical analysis
  - Software scripts and visualization

SUPPLEMENTAL INFORMATION

Supplemental information can be found online at https://doi.org/10.1016/j.celrep.2022.111013.

ACKNOWLEDGMENTS

The authors are grateful to the study participants. We thank the CRCHUM BSL3 and Flow Cytometry platforms for technical assistance, Dr. Johanne Poudrier for advices and discussions, Dr. Stefan Pöhlmann (Georg-August University, Germany) for the plasmid coding for SARS-CoV-2 S glycoproteins, and Dr. M. Gordon Joyce (U.S. MHRP) for the monoclonal antibody CR3022. This work was supported by an FRQS Merit Research Scholar award to D.E.K., the Fondation du CHUM, le Ministère de l'Économie et de l'Innovation du Québec, Program de soutient aux organismes de recherche et d'innovation (to A.F.), a CIHR operating grant #178344 (D.E.K. and A.F.), a foundation grant #352417 (A.F.), a CIHR operating Pandemic and Health Emergencies Research grant #177958(A.F.), and an Exceptional Fund COVID-19 from the Canada Foundation for Innovation (CFI) #41027 to A.F. and D.E.K. The Symphony flow cytometer was funded by a John R. Evans Leaders Fund Leader Fund from the Canada Foundation for Innovation (#37521 to D.E.K.) and the Fondation Sclérodermie Québec. A.F. is the recipient of Canada Research Chair on Retroviral Entry no. RCHS0235 950-232424. A.P. holds a Canada Research Chair in Multiple Sclerosis and the Power Corporation of Canada Chair of Université de Montréal. V.M.L. is supported by an FRQS Junior 1 salary award, G.S. by a scholarship from the Department of Microbiology, Infectious Disease and Immunology of the University of Montréal, G.B.B. by an FRQS doctoral fellowship, R.G. and A.L. by a MITACS Accélération postdoctoral fellowship, and J.P. by a CIHR doctoral fellowship. The funders had no role in study design, data collection and analysis, decision to publish, or preparation of the manuscript.

AUTHOR CONTRIBUTIONS

M.N., M.D., A.F., and D.E.K. designed the studies. M.N., G.S., A.N., N.B., and M.L. performed B cell and T cell assays. J.P. generated the B cell probes. M.N., M.D., G.S., A.N., and O.T. performed and analyzed the B and T cell experiments. J.N. contributed to the T cell assay design. O.T. performed unsupervised clustering analyses. L.M., A.T., G.B.-B., D.V., S.Y.G., M.B., R.G., J.P., C.B., G.G.-L., and J.R. performed ELISA, ADCC, flow cytometry, avidity, and neutralization assays. A.L., C.B., G.G.-L., H.M., L.G., C.M., P.A., G.-G.O.-D., C.T., and V.M.-L. secured and processed blood samples. G.G. produced and purified proteins. A.P. provided intellectual input. J.B. and R.L.-B. generated and applied the linear mixed models for statistical comparison. M.N., M.D., and D.E.K. wrote the manuscript. Every author has read, edited, and approved the final manuscript.

DECLARATION OF INTERESTS

The authors declare no competing interests.

Received: January 4, 2022
Revised: April 27, 2022
Accepted: June 6, 2022
Published: June 28, 2022

REFERENCES

Anand, S.P., Prévost, J., Nayrac, M., Beaudoin-Bussières, G., Benlarbi, M., Gasser, R., Brassard, N., Laumaea, A., Gong, S.Y., Bourassa, C., et al. (2021). Longitudinal analysis of humoral immunity against SARS-CoV-2 Spike in convalescent individuals up to 8 months post-symptom onset. Medicine *2*, 100290. https://doi.org/10.1016/j.xcrm.2021.100290.

Anderson, E.J., Rouphael, N.G., Widge, A.T., Jackson, L.A., Roberts, P.C., Makhene, M., Chappell, J.D., Denison, M.R., Stevens, L.J., Pruijssers, A.J., et al. (2020). Safety and immunogenicity of SARS-CoV-2 mRNA-1273 vaccine

(C) PCA subanalyses divided by time points. Only complete datasets could be loaded in the PCA analysis. The numbers of participants by PCA are shown in each plot.
(D) Box-and-whisker plots of the PC1 and PC2 between group are shown with Mann-Whitney tests.
(E) Spearman correlations between each individual immune feature and PC1 (*$p < 0.05$, **$p < 0.01$, ***$p < 0.001$).

in older adults. N. Engl. J. Med. *383*, 2427–2438. https://doi.org/10.1056/NEJMoa2028436.

Apostolidis, S.A., Kakara, M., Painter, M.M., Goel, R.R., Mathew, D., Lenzi, K., Rezk, A., Patterson, K.R., Espinoza, D.A., Kadri, J.C., et al. (2021). Cellular and humoral immune responses following SARS-CoV-2 mRNA vaccination in patients with multiple sclerosis on anti-CD20 therapy. Nature medicine *27*, 1990–2001. https://doi.org/10.1038/s41591-021-01507-2.

Aujla, S.J., Chan, Y.R., Zheng, M., Fei, M., Askew, D.J., Pociask, D.A., Reinhart, T.A., McAllister, F., Edeal, J., Gaus, K., et al. (2008). IL-22 mediates mucosal host defense against Gram-negative bacterial pneumonia. Nature medicine *14*, 275–281. https://doi.org/10.1038/nm1710.

Baden, L.R., El Sahly, H.M., Essink, B., Kotloff, K., Frey, S., Novak, R., Diemert, D., Spector, S.A., Rouphael, N., Creech, C.B., et al. (2021). Efficacy and safety of the mRNA-1273 SARS-CoV-2 vaccine. N. Engl. J. Med. *384*, 403–416. https://doi.org/10.1056/NEJMoa2035389.

Bange, E.M., Han, N.A., Wileyto, P., Kim, J.Y., Gouma, S., Robinson, J., Greenplate, A.R., Hwee, M.A., Porterfield, F., Owoyemi, O., et al. (2021). CD8(+) T cells contribute to survival in patients with COVID-19 and hematologic cancer. Nature medicine *27*, 1280–1289. https://doi.org/10.1038/s41591-021-01386-7.

Beaudoin-Bussières, G., Laumaea, A., Anand, S.P., Prévost, J., Gasser, R., Goyette, G., Medjahed, H., Perreault, J., Tremblay, T., Lewin, A., et al. (2020). Decline of humoral responses against SARS-CoV-2 Spike in convalescent individuals. mBio *11*. https://doi.org/10.1128/mBio.02590-20.

Becht, E., McInnes, L., Healy, J., Dutertre, C.A., Kwok, I.W.H., Ng, L.G., Ginhoux, F., and Newell, E.W. (2018). Dimensionality reduction for visualizing single-cell data using UMAP. Nat. Biotechnol. *37*, 38–44. https://doi.org/10.1038/nbt.4314.

Carazo, S., Talbot, D., Boulianne, N., Brisson, M., Gilca, R., Deceuninck, G., Brousseau, N., Drolet, M., Ouakki, M., Sauvageau, C., et al. (2021). Single-dose mRNA vaccine effectiveness against SARS-CoV-2 in healthcare workers extending 16 weeks post-vaccination: a test-negative design from Quebec, Canada. Clin. Infect. Dis. *74* (*11*), ciab739, an official publication of the Infectious Diseases Society of America. https://doi.org/10.1093/cid/ciab739.

Chatterjee, D., Tauzin, A., Marchitto, L., Gong, S.Y., Boutin, M., Bourassa, C., Beaudoin-Bussières, G., Bo, Y., Ding, S., Laumaea, A., et al. (2022). SARS-CoV-2 Omicron Spike recognition by plasma from individuals receiving BNT162b2 mRNA vaccination with a 16-week interval between doses. Cell Rep. *38*, 110429. https://doi.org/10.1016/j.celrep.2022.110429.

Crotty, S. (2019). T follicular helper cell biology: a decade of discovery and diseases. Immunity *50*, 1132–1148. https://doi.org/10.1016/j.immuni.2019.04.011.

da Silva Antunes, R., Babor, M., Carpenter, C., Khalil, N., Cortese, M., Mentzer, A.J., Seumois, G., Petro, C.D., Purcell, L.A., Vijayanand, P., et al. (2018). Th1/Th17 polarization persists following whole-cell pertussis vaccination despite repeated acellular boosters. J. Clin. Invest. *128*, 3853–3865. https://doi.org/10.1172/JCI121309.

Darrah, P.A., Patel, D.T., De Luca, P.M., Lindsay, R.W.B., Davey, D.F., Flynn, B.J., Hoff, S.T., Andersen, P., Reed, S.G., Morris, S.L., et al. (2007). Multifunctional TH1 cells define a correlate of vaccine-mediated protection against Leishmania major. Nature medicine *13*, 843–850. https://doi.org/10.1038/nm1592.

Day, C.E., Zhang, S.D., Riley, J., Gant, T., Wardlaw, A.J., and Guillen, C. (2009). A novel method for isolation of human lung T cells from lung resection tissue reveals increased expression of GAPDH and CXCR6. J. Immunol. Methods *342*, 91–97. https://doi.org/10.1016/j.jim.2008.12.001.

Dickerman, B.A., Gerlovin, H., Madenci, A.L., Kurgansky, K.E., Ferolito, B.R., Figueroa Muñiz, M.J., Gagnon, D.R., Gaziano, J.M., Cho, K., Casas, J.P., and Hernán, M.A. (2022). Comparative effectiveness of BNT162b2 and mRNA-1273 vaccines in U.S. Veterans. N. Engl. J. Med. *386*, 105–115. https://doi.org/10.1056/NEJMoa2115463.

Earle, K.A., Ambrosino, D.M., Fiore-Gartland, A., Goldblatt, D., Gilbert, P.B., Siber, G.R., Dull, P., and Plotkin, S.A. (2021). Evidence for antibody as a protective correlate for COVID-19 vaccines. Vaccine *39*, 4423–4428. https://doi.org/10.1016/j.vaccine.2021.05.063.

Efrati, S., Catalogna, M., Abu Hamad, R., Hadanny, A., Bar-Chaim, A., Benveniste-Levkovitz, P., and Levtzion-Korach, O. (2021). Safety and humoral responses to BNT162b2 mRNA vaccination of SARS-CoV-2 previously infected and naive populations. Sci. Rep. *11*, 16543. https://doi.org/10.1038/s41598-021-96129-6.

Gilbert, P.B., Montefiori, D.C., McDermott, A.B., Fong, Y., Benkeser, D., Deng, W., Zhou, H., Houchens, C.R., Martins, K., Jayashankar, L., et al. (2022). Immune correlates analysis of the mRNA-1273 COVID-19 vaccine efficacy clinical trial. Science *375*, 43–50. https://doi.org/10.1126/science.abm3425.

Goel, R.R., Painter, M.M., Apostolidis, S.A., Mathew, D., Meng, W., Rosenfeld, A.M., Lundgreen, K.A., Reynaldi, A., Khoury, D.S., Pattekar, A., et al. (2021). mRNA vaccines induce durable immune memory to SARS-CoV-2 and variants of concern. Science *374*, eabm0829. https://doi.org/10.1126/science.abm0829.

Grifoni, A., Weiskopf, D., Ramirez, S.I., Mateus, J., Dan, J.M., Moderbacher, C.R., Rawlings, S.A., Sutherland, A., Premkumar, L., Jadi, R.S., et al. (2020). Targets of T Cell Responses to SARS-CoV-2 Coronavirus in Humans with COVID-19 Disease and Unexposed Individuals. Cell *181*, 1489–1501, e1415. https://doi.org/10.1016/j.cell.2020.05.015.

Grunau, B., Goldfarb, D.M., Asamoah-Boaheng, M., Golding, L., Kirkham, T.L., Demers, P.A., and Lavoie, P.M. (2022). Immunogenicity of extended mRNA SARS-CoV-2 vaccine dosing intervals. JAMA *327*, 279–281. https://doi.org/10.1001/jama.2021.21921.

Hicks, J., Klumpp-Thomas, C., Kalish, H., Shunmugavel, A., Mehalko, J., Denson, J.P., Snead, K.R., Drew, M., Corbett, K.S., Graham, B.S., et al. (2021). Serologic cross-reactivity of SARS-CoV-2 with endemic and seasonal betacoronaviruses. J. Clin. Immunol. *41*, 906–913. https://doi.org/10.1007/s10875-021-00997-6.

Hoffmann, M., Kleine-Weber, H., Schroeder, S., Krüger, N., Herrler, T., Erichsen, S., Schiergens, T.S., Herrler, G., Wu, N.H., Nitsche, A., et al. (2020). SARS-CoV-2 cell entry depends on ACE2 and TMPRSS2 and is blocked by a clinically proven protease inhibitor. Cell *181*, 271–280.e8, e278. https://doi.org/10.1016/j.cell.2020.02.052.

Jenks, S.A., Cashman, K.S., Zumaquero, E., Marigorta, U.M., Patel, A.V., Wang, X., Tomar, D., Woodruff, M.C., Simon, Z., Bugrovsky, R., et al. (2018). Distinct effector B cells induced by unregulated toll-like receptor 7 contribute to pathogenic responses in systemic lupus erythematosus. Immunity *49*, 725–739.e6, e726. https://doi.org/10.1016/j.immuni.2018.08.015.

Khader, S.A., Bell, G.K., Pearl, J.E., Fountain, J.J., Rangel-Moreno, J., Cilley, G.E., Shen, F., Eaton, S.M., Gaffen, S.L., Swain, S.L., et al. (2007). IL-23 and IL-17 in the establishment of protective pulmonary CD4+ T cell responses after vaccination and during Mycobacterium tuberculosis challenge. Nat. Immunol. *8*, 369–377. https://doi.org/10.1038/ni1449.

Klumpp-Thomas, C., Kalish, H., Drew, M., Hunsberger, S., Snead, K., Fay, M.P., Mehalko, J., Shunmugavel, A., Wall, V., Frank, P., et al. (2021). Standardization of ELISA protocols for serosurveys of the SARS-CoV-2 pandemic using clinical and at-home blood sampling. Nat. Commun. *12*, 113. https://doi.org/10.1038/s41467-020-20383-x.

Krammer, F. (2020). SARS-CoV-2 vaccines in development. Nature *586*, 516–527. https://doi.org/10.1038/s41586-020-2798-3.

Laidlaw, B.J., Craft, J.E., and Kaech, S.M. (2016). The multifaceted role of CD4(+) T cells in CD8(+) T cell memory. Nat. Rev. Immunol. *16*, 102–111. https://doi.org/10.1038/nri.2015.10.

Lederer, K., Castaño, D., Gómez Atria, D., Oguin, T.H., 3rd, Wang, S., Manzoni, T.B., Muramatsu, H., Hogan, M.J., Amanat, F., Cherubin, P., et al. (2020). SARS-CoV-2 mRNA vaccines foster potent antigen-specific germinal center responses associated with neutralizing antibody generation. Immunity *53*, 1281–1295.e5, e1285. https://doi.org/10.1016/j.immuni.2020.11.009.

Levine, J.H., Simonds, E.F., Bendall, S.C., Davis, K.L., Amir, E.a., Amir el, A.D., Tadmor, M.D., Litvin, O., Fienberg, H.G., Jager, A., et al. (2015). Data-driven phenotypic dissection of AML reveals progenitor-like cells that correlate with prognosis. Cell *162*, 184–197. https://doi.org/10.1016/j.cell.2015.05.047.

Loyal, L., Braun, J., Henze, L., Kruse, B., Dingeldey, M., Reimer, U., Kern, F., Schwarz, T., Mangold, M., Unger, C., et al. (2021). Cross-reactive CD4(+) T cells enhance SARS-CoV-2 immune responses upon infection and vaccination. Science *374*, eabh1823. https://doi.org/10.1126/science.abh1823.

Mateus, J., Grifoni, A., Tarke, A., Sidney, J., Ramirez, S.I., Dan, J.M., Burger, Z.C., Rawlings, S.A., Smith, D.M., Phillips, E., et al. (2020). Selective and cross-reactive SARS-CoV-2 T cell epitopes in unexposed humans. Science *370*, 89–94. https://doi.org/10.1126/science.abd3871.

Maucourant, C., Filipovic, I., Ponzetta, A., Aleman, S., Cornillet, M., Hertwig, L., Strunz, B., Lentini, A., Reinius, B., Brownlie, D., et al. (2020). Natural killer cell immunotypes related to COVID-19 disease severity. Science immunology *5*, eabd6832. https://doi.org/10.1126/sciimmunol.abd6832.

Moore, K.W., Rogers, J., Hunkapiller, T., Early, P., Nottenburg, C., Weissman, I., Bazin, H., Wall, R., and Hood, L.E. (1981). Expression of IgD may use both DNA rearrangement and RNA splicing mechanisms. Proc. Natl. Acad. Sci. U. S. A. *78*, 1800–1804. https://doi.org/10.1073/pnas.78.3.1800.

Morgan, X.C., Kabakchiev, B., Waldron, L., Tyler, A.D., Tickle, T.L., Milgrom, R., Stempak, J.M., Gevers, D., Xavier, R.J., Silverberg, M.S., and Huttenhower, C. (2015). Associations between host gene expression, the mucosal microbiome, and clinical outcome in the pelvic pouch of patients with inflammatory bowel disease. Genome Biol. *16*, 67. https://doi.org/10.1186/s13059-015-0637-x.

Morou, A., Brunet-Ratnasingham, E., Dubé, M., Charlebois, R., Mercier, E., Darko, S., Brassard, N., Nganou-Makamdop, K., Arumugam, S., Gendron-Lepage, G., et al. (2019). Altered differentiation is central to HIV-specific CD4(+) T cell dysfunction in progressive disease. Nat. Immunol. *20*, 1059–1070. https://doi.org/10.1038/s41590-019-0418-x.

Nakanishi, Y., Lu, B., Gerard, C., and Iwasaki, A. (2009). CD8(+) T lymphocyte mobilization to virus-infected tissue requires CD4(+) T-cell help. Nature *462*, 510–513. https://doi.org/10.1038/nature08511.

Niessl, J., Baxter, A.E., Mendoza, P., Jankovic, M., Cohen, Y.Z., Butler, A.L., Lu, C.L., Dubé, M., Shimeliovich, I., Gruell, H., et al. (2020a). Combination anti-HIV-1 antibody therapy is associated with increased virus-specific T cell immunity. Nature medicine *26*, 222–227. https://doi.org/10.1038/s41591-019-0747-1.

Niessl, J., Baxter, A.E., Morou, A., Brunet-Ratnasingham, E., Sannier, G., Gendron-Lepage, G., Richard, J., Delgado, G.G., Brassard, N., Turcotte, I., et al. (2020b). Persistent expansion and Th1-like skewing of HIV-specific circulating T follicular helper cells during antiretroviral therapy. EBioMedicine *54*, 102727. https://doi.org/10.1016/j.ebiom.2020.102727.

O'Shea, J.J., and Paul, W.E. (2010). Mechanisms underlying lineage commitment and plasticity of helper CD4+ T cells. Science *327*, 1098–1102. https://doi.org/10.1126/science.1178334.

Oberhardt, V., Luxenburger, H., Kemming, J., Schulien, I., Ciminski, K., Giese, S., Csernalabics, B., Lang-Meli, J., Janowska, I., Staniek, J., et al. (2021). Rapid and stable mobilization of CD8(+) T cells by SARS-CoV-2 mRNA vaccine. Nature *597*, 268–273. https://doi.org/10.1038/s41586-021-03841-4.

Painter, M.M., Mathew, D., Goel, R.R., Apostolidis, S.A., Pattekar, A., Kuthuru, O., Baxter, A.E., Herati, R.S., Oldridge, D.A., Gouma, S., et al. (2021). Rapid induction of antigen-specific CD4(+) T cells is associated with coordinated humoral and cellular immunity to SARS-CoV-2 mRNA vaccination. Immunity *54*, 2133–2142.e3, e2133. https://doi.org/10.1016/j.immuni.2021.08.001.

Paltiel, A.D., Zheng, A., and Schwartz, J.L. (2021). Speed versus efficacy: quantifying potential tradeoffs in COVID-19 vaccine deployment. Ann. Intern. Med. *174*, 568–570. https://doi.org/10.7326/M20-7866.

Parry, H., Bruton, R., Stephens, C., Brown, K., Amirthalingam, G., Otter, A., Hallis, B., Zuo, J., and Moss, P. (2021). Differential immunogenicity of BNT162b2 or ChAdOx1 vaccines after extended-interval homologous dual vaccination in older people. Immun. Ageing : I & A *18*, 34. https://doi.org/10.1186/s12979-021-00246-9.

Payne, R.P., Longet, S., Austin, J.A., Skelly, D.T., Dejnirattisai, W., Adele, S., Meardon, N., Faustini, S., Al-Taei, S., Moore, S.C., et al. (2021). Immunogenicity of standard and extended dosing intervals of BNT162b2 mRNA vaccine. Cell *184*, 5699–5714.e11, e5611. https://doi.org/10.1016/j.cell.2021.10.011.

Polack, F.P., Thomas, S.J., Kitchin, N., Absalon, J., Gurtman, A., Lockhart, S., Perez, J.L., Pérez Marc, G., Moreira, E.D., Zerbini, C., et al. (2020). Safety and efficacy of the BNT162b2 mRNA Covid-19 vaccine. N. Engl. J. Med. *383*, 2603–2615. https://doi.org/10.1056/NEJMoa2034577.

Prendecki, M., Clarke, C., Brown, J., Cox, A., Gleeson, S., Guckian, M., Randell, P., Pria, A.D., Lightstone, L., Xu, X.N., et al. (2021). Effect of previous SARS-CoV-2 infection on humoral and T-cell responses to single-dose BNT162b2 vaccine. Lancet *397*, 1178–1181. https://doi.org/10.1016/S0140-6736(21)00502-X.

Prevost, J., Gasser, R., Beaudoin-Bussieres, G., Richard, J., Duerr, R., Laumaea, A., Anand, S.P., Goyette, G., Benlarbi, M., Ding, S., et al. (2020). Cross-sectional evaluation of humoral responses against SARS-CoV-2 Spike. Preprint at bioRxiv, the preprint server for biology. https://doi.org/10.1101/2020.06.08.140244.

Quintelier, K., Couckuyt, A., Emmaneel, A., Aerts, J., Saeys, Y., and Van Gassen, S. (2021). Analyzing high-dimensional cytometry data using FlowSOM. Nat. Protoc. *16*, 3775–3801. https://doi.org/10.1038/s41596-021-00550-0.

Rodda, L.B., Morawski, P.A., Pruner, K.B., Fahning, M.L., Howard, C.A., Franko, N., Logue, J., Eggenberger, J., Stokes, C., Golez, I., et al. (2022). Imprinted SARS-CoV-2-specific memory lymphocytes define hybrid immunity. Cell *185*, 1588–1601.e14. https://doi.org/10.1016/j.cell.2022.03.018.

Ruschil, C., Gabernet, G., Lepennetier, G., Heumos, S., Kaminski, M., Hracsko, Z., Irmler, M., Beckers, J., Ziemann, U., Nahnsen, S., et al. (2020). Specific induction of double negative B cells during protective and pathogenic immune responses. Front. Immunol. *11*, 606338. https://doi.org/10.3389/fimmu.2020.606338.

Sahin, U., Muik, A., Derhovanessian, E., Vogler, I., Kranz, L.M., Vormehr, M., Baum, A., Pascal, K., Quandt, J., Maurus, D., et al. (2020). COVID-19 vaccine BNT162b1 elicits human antibody and TH1 T cell responses. Nature *586*, 594–599. https://doi.org/10.1038/s41586-020-2814-7.

Shrock, E., Fujimura, E., Kula, T., Timms, R.T., Lee, I.H., Leng, Y., Robinson, M.L., Sie, B.M., Li, M.Z., Chen, Y., et al. (2020). Viral epitope profiling of COVID-19 patients reveals cross-reactivity and correlates of severity. Science *370*. https://doi.org/10.1126/science.abd4250.

Skowronski, D.M., and De Serres, G. (2021). Safety and efficacy of the BNT162b2 mRNA Covid-19 vaccine. N. Engl. J. Med. *384*, 1576–1577. https://doi.org/10.1056/NEJMc2036242.

Skowronski, D.M., Setayeshgar, S., Febriani, Y., Ouakki, M., Zou, M., Talbot, D., Prystajecky, N., Tyson, J.R., Gilca, R., Brousseau, N., et al. (2021). Two-dose SARS-CoV-2 vaccine effectiveness with mixed schedules and extended dosing intervals: test-negative design studies from British Columbia and Quebec, Canada. Preprint at medRxiv, the preprint server for health sciences. https://doi.org/10.1101/2021.10.26.21265397.

Stamatatos, L., Czartoski, J., Wan, Y.H., Homad, L.J., Rubin, V., Glantz, H., Neradilek, M., Seydoux, E., Jennewein, M.F., MacCamy, A.J., et al. (2021). mRNA vaccination boosts cross-variant neutralizing antibodies elicited by SARS-CoV-2 infection. Science *372* (*6549*), eabg9175. https://doi.org/10.1126/science.abg9175.

Tangye, S.G., Liu, Y.J., Aversa, G., Phillips, J.H., and de Vries, J.E. (1998). Identification of functional human splenic memory B cells by expression of CD148 and CD27. J. Exp. Med. *188*, 1691–1703. https://doi.org/10.1084/jem.188.9.1691.

Tauzin, A., Gong, S.Y., Beaudoin-Bussières, G., Vézina, D., Gasser, R., Nault, L., Marchitto, L., Benlarbi, M., Chatterjee, D., Nayrac, M., et al. (2022). Strong humoral immune responses against SARS-CoV-2 Spike after BNT162b2 mRNA vaccination with a 16-week interval between doses. Cell host & microbe *30*, 97–109.e5. https://doi.org/10.1016/j.chom.2021.12.004.

Tauzin, A., Nayrac, M., Benlarbi, M., Gong, S.Y., Gasser, R., Beaudoin-Bussières, G., Brassard, N., Laumaea, A., Vézina, D., Prévost, J., et al. (2021b). A single dose of the SARS-CoV-2 vaccine BNT162b2 elicits Fc-mediated antibody effector functions and T cell responses. Cell host & microbe *29*, 1137–1150.e6, e1136. https://doi.org/10.1016/j.chom.2021.06.001.

Thomas, S.J., Moreira, E.D., Jr., Kitchin, N., Absalon, J., Gurtman, A., Lockhart, S., Perez, J.L., Pérez Marc, G., Polack, F.P., Zerbini, C., et al. (2021).

Safety and efficacy of the BNT162b2 mRNA Covid-19 vaccine through 6 months. N. Engl. J. Med. *385*, 1761–1773. https://doi.org/10.1056/NEJMoa2110345.

Tuite, A.R., Zhu, L., Fisman, D.N., and Salomon, J.A. (2021). Alternative dose allocation strategies to increase benefits from constrained COVID-19 vaccine supply. Ann. Intern. Med. *174*, 570–572. https://doi.org/10.7326/M20-8137.

Urbanowicz, R.A., Tsoleridis, T., Jackson, H.J., Cusin, L., Duncan, J.D., Chappell, J.G., Tarr, A.W., Nightingale, J., Norrish, A.R., Ikram, A., et al. (2021). Two doses of the SARS-CoV-2 BNT162b2 vaccine enhance antibody responses to variants in individuals with prior SARS-CoV-2 infection. Sci. Transl. Med. *13*, eabj0847. https://doi.org/10.1126/scitranslmed.abj0847.

Walls, A.C., Park, Y.J., Tortorici, M.A., Wall, A., McGuire, A.T., and Veesler, D. (2020). Structure, function, and antigenicity of the SARS-CoV-2 Spike glycoprotein. Cell *181*, 281–292.e6, e286. https://doi.org/10.1016/j.cell.2020.02.058.

Wei, C., Anolik, J., Cappione, A., Zheng, B., Pugh-Bernard, A., Brooks, J., Lee, E.H., Milner, E.C.B., and Sanz, I. (2007). A new population of cells lacking expression of CD27 represents a notable component of the B cell memory compartment in systemic lupus erythematosus. J. Immunol. *178*, 6624–6633. https://doi.org/10.4049/jimmunol.178.10.6624.

Wurm, H., Attfield, K., Iversen, A.K., Gold, R., Fugger, L., and Haghikia, A. (2020). Recovery from COVID-19 in a B-cell-depleted multiple sclerosis patient. Mult. Scler. *26*, 1261–1264. https://doi.org/10.1177/1352458520943791.

Zollner, A., Watschinger, C., Rössler, A., Farcet, M.R., Penner, A., Böhm, V., Kiechl, S.J., Stampfel, G., Hintenberger, R., Tilg, H., et al. (2021). B and T cell response to SARS-CoV-2 vaccination in health care professionals with and without previous COVID-19. EBioMedicine *70*, 103539. https://doi.org/10.1016/j.ebiom.2021.103539.

STAR★METHODS

KEY RESOURCES TABLE

REAGENT or RESOURCE	SOURCE	IDENTIFIER
Antibodies		
UCHT1 (BUV395) [Human anti-CD3]	BD Biosciences	Cat#563546 ; Lot:9058566 ; RRID:AB_2744387
UCHT1 (BUV496) [Human anti-CD3]	BD Biosciences	Cat#612941 ; Lot:1022424 ; RRID:AB_2870222
L200 (BV711) [Human anti-CD4]	BD Biosciences	Cat#563913 ; Lot:03000025; RRID:AB_2738484
SK3 (BB630) [Human anti-CD4]	BD Biosciences	Cat#624294 CUSTOM ; Lot:0289566
RPA-T8 (BV570) [Human anti-CD8]	Biolegend	Cat#301037 ; Lot:B281322 ; RRID:AB_10933259
M5E2 (BUV805) [Human anti-CD14]	BD Biosciences	Cat#612902 ; Lot:0262150 ; RRID:AB_2870189
M5E2 (BV480) [Human anti-CD14]	BD Biosciences	Cat#746304; Lot : 9133961 ; RRID:AB_2743629
3G8 (BV650) [Human anti-CD16]	Biolegend	Cat#302042 ; Lot:B323847 ; RRID:AB_2563801
HIB19 (APC-eFluor780) [Human anti-CD19]	Thermo Fisher Scientific	Cat#47-0199 ; Lot:2145095 ; RRID:AB_1582231
HIB19 (BV480) [Human anti-CD19]	BD Biosciences	Cat#746457 ; Lot:1021649 ; RRID:AB_2743759
HI100 (PerCP Cy5.5) [Human anti-CD45RA]	BD Biosciences	Cat#563429 ; Lot:8332746 ; RRID:AB_2738199
NCAM16.2 (BUV737) [Human anti-CD56]	BD Biosciences	Cat#564448 ; Lot:8288818 ; RRID:AB_2744432
FN50 (PerCP-eFluor710) [Human anti-CD69]	Thermo Fisher Scientific	Cat#46-0699-42 ; Lot:1920361 ; RRID:AB_2573694
FN50 (BV650) [Human anti-CD69]	Biolegend	Cat# 310934 ; Lot:B303462 ; RRID:AB_2563158
H4A3 (BV786) [Human anti-CD107A]	BD Biosciences	Cat#563869 ; Lot:8144866 ; RRID:AB_2738458
ACT35 (APC) [Human anti-CD134 (OX40)]	BD Biosciences	Cat#563473 ; Lot:1015537 ; RRID:AB_2738230
4B4-1 (PE-Dazzle 594) [Human anti-CD137 (4-1BB)]	Biolegend	Cat# 309826 ; Lot:B253152 ; RRID:AB_2566260
TRAP1 (BV421) [Human anti-CD154 (CD40L)]	BD Biosciences	Cat#563886 ; Lot:9037850 ; RRID:AB_2738466
TRAP1 (PE) [Human anti-CD154 (CD40L)]	BD Biosciences	Cat#555700 ; Lot:7086896 ; RRID:AB_396050
J25D4 (BV421) [Human anti-CD185 (CXCR5)]	Biolegend	Cat# 356920 ; Lot:B325837 ; RRID:AB_2562303
B27 (PECy7) [Human anti-IFN-γ]	BD Biosciences	Cat#557643 ; Lot:8256597 ; RRID:AB_396760
MQ1-17H12 (PE-Dazzle594) [Human anti-IL-2]	Biolegend	Cat#500344 ; Lot:B2261476 ; RRID:AB_2564091
JES3-9D7 (PE) [Human anti-IL-10]	BD Biosciences	Cat#554498 ; Lot:8198773 ; RRID:AB_395434
eBio64CAP17 (eFluor660) [Human anti-IL-17A]	Thermo Fisher Scientific	Cat#50-7179-42 ; Lot:2151998 ; RRID:AB_11149126

(*Continued on next page*)

Continued

REAGENT or RESOURCE	SOURCE	IDENTIFIER
Mab11 (Alexa Fluor 488) [Human anti-TNF-α]	Biolegend	Cat#502915 ; Lot:B285221 ; RRID:AB_493121
LIVE/DEAD Fixable dead cell	Thermo Fisher Scientific	L34960
Biological samples		
SARS-CoV-2 naive donor blood samples	N/A	
SARS-CoV-2 prior infection donor blood samples	N/A	
Chemicals, peptides, and recombinant proteins		
PepMix™ SARS-CoV-2 (Spike Glycoprotein)	JPT	Cat#PM-WCPV-S-1
Staphylococcal Enterotoxin B (SEB)	Toxin technology	Cat#BT202
Software and algorithms		
Flow Jo v10.8.0	Flow Jo	https://www.flowjo.com
GraphPad Prism v8.4.1	GraphPad	https://www.graphpad.com
R studio v4.1.0	R studio	https://rstudio.com
R codes scripted	Github	https://github.com/otastet/Nayrac_et_al
Deposited data		
Table S4	Mendeley database: DOI: 10.17632/d5mg48z55p.1	

RESOURCE AVAILABILITY

Lead contact

Further information and requests for resources and reagents should be directed to and will be fulfilled by the lead contact, Daniel E. Kaufmann (daniel.kaufmann@umontreal.ca).

Materials availability

All unique reagents generated during this study are available from the lead contact upon a material transfer agreement (MTA).

Data and code availability

The published article includes all datasets generated and analyzed for this study. All datasets are also available at Mendeley Data: https://doi.org/10.17632/d5mg48z55p.1. Further information and requests for resources and reagents should be directed to and will be fulfilled by the Lead Contact Author (daniel.kaufmann@umontreal.ca).

We adapted R codes scripted to perform unsupervised analyzes on B and T cells from SARS-CoV-2 naive and previously-infected individuals. All original codes have been deposited at Github and are publicly available as of the date of publication. URL link is listed in the key resources table.

Any additional information required to reanalyze the data reported in this paper is available from the Lead Contact Author upon request (daniel.kaufmann@umontreal.ca).

EXPERIMENTAL MODEL AND SUBJECT DETAILS

Ethics statement

All work was conducted in accordance with the Declaration of Helsinki in terms of informed consent and approval by an appropriate institutional board. Blood samples were obtained from donors who consented to participate in this research project at the CHUM (19.381). Plasma and PBMCs were isolated by centrifugation and Ficoll gradient, and samples stored at −80°C and in liquid nitrogen, respectively, until use.

Participants

No specific criteria such as number of patients (sample size), clinical or demographic were used for inclusion, beyond PCR confirmed SARS-CoV-2 infection in adults enrolled in the previously infected cohorts. Clinical data are summarized in Table 1.

PBMCs and plasma collection

PBMCs were isolated from blood samples by Ficoll density gradient centrifugation and cryopreserved in liquid nitrogen until use. Plasma was collected, heat-inactivated for 1 h at 56°C and stored at −80°C until ready to use in subsequent experiments. Plasma

from uninfected donors collected before the pandemic were used as negative controls and used to calculate the seropositivity threshold in our ELISA and ADCC assays.

Cell lines

293T human embryonic kidney and HOS cells (obtained from ATCC) were maintained at 37°C under 5% CO_2 in Dulbecco's modified Eagle's medium (DMEM) (Wisent) containing 5% fetal bovine serum (FBS) (VWR) and 100 μg/mL of penicillin-streptomycin (Wisent). CEM.NKr CCR5+ cells (NIH AIDS reagent program) were maintained at 37°C under 5% CO_2 in Roswell Park Memorial Institute (RPMI) 1,640 medium (Gibco) containing 10% FBS and 100 μg/mL of penicillin-streptomycin. 293T-ACE2 cell line was previously reported (Prevost et al., 2020). HOS and CEM.NKr CCR5+ cells stably expressing the SARS-CoV-2 S glycoproteins (CEM.NKr.Spike cells) were previously reported (Anand et al., 2021).

METHOD DETAILS

Protein expression and purification

FreeStyle 293F cells (Thermo Fisher Scientific) were grown in FreeStyle 293F medium (Thermo Fisher Scientific) to a density of 1×10^6 cells/mL at 37°C with 8% CO_2 with regular agitation (150 rpm). Cells were transfected with a plasmid coding for SARS-CoV-2 S RBD using ExpiFectamine 293 transfection reagent, as directed by the manufacturer (Invitrogen) (Beaudoin-Bussieres et al., 2020; Prevost et al., 2020). One week later, cells were pelleted and discarded. Supernatants were filtered using a 0.22 μm filter (Thermo Fisher Scientific). The recombinant RBD proteins were purified by nickel affinity columns, as directed by the manufacturer (Thermo Fisher Scientific). The RBD preparations were dialyzed against phosphate-buffered saline (PBS) and stored in aliquots at −80°C until further use. To assess purity, recombinant proteins were loaded on SDS-PAGE gels and stained with Coomassie Blue.

RBD-specific IgG levels and avidity measured by enzyme-linked immunosorbent assay (ELISA)

The SARS-CoV-2 RBD ELISA assay was used to measure the level of RBD-specific IgG, as previously described (Beaudoin-Bussieres et al., 2020; Prevost et al., 2020). Briefly, recombinant SARS-CoV-2 RBD protein was prepared in PBS (2.5 μg/mL) and adsorbed to plates overnight at 4°C. Coated wells were subsequently blocked with blocking buffer then washed. CR3022 monoclonal Ab (50 ng/mL) at 1/250, 1/500, 1/1,250, 1/2,500, 1/5,000, 1/10,000, 1/20,000 dilutions of plasma from SARS-CoV-2-naive or previously infected donors were prepared in a diluted solution of blocking buffer and incubated with the RBD-coated wells. Plates were washed followed by incubation with the respective secondary Abs. Area Under the Curve (AUC) was calculated by using GraphPad. To calculate the RBD-avidity index, we performed a stringent ELISA where the plate was washed with washing buffer supplemented 8M urea. The binding of CR3022 IgG and plasma was quantified with HRP-conjugated antibodies specific for the Fc region of human IgG. HRP enzyme activity was determined after the addition of a 1:1 mix of Western Lightning oxidizing and luminol reagents (Perkin Elmer Life Sciences). Light emission was measured with a LB942 TriStar luminometer (Berthold Technologies).

Spike IgG levels measured by cell-based ELISA (CBE)

Detection of the trimeric SARS-CoV-2 S at the surface of HOS cells was performed by a previously described cell-based enzyme-linked immunosorbent assay (ELISA) (Anand et al., 2021). Briefly, parental HOS cells or HOS-Spike cells by Spike specific IgG were seeded in 96-well plates (6×10^4 cells per well) overnight. Cells were blocked with blocking buffer (10 mg/mL nonfat dry milk, 1.8 mM $CaCl_2$, 1 mM $MgCl_2$, 25 mM Tris [pH 7.5], and 140 mM NaCl) for 30 min. CR3022 mAb (1 μg/mL) or plasma (at a dilution of 1/250) were prepared in blocking buffer and incubated with the cells for 1 h at room temperature. Respective HRP-conjugated anti-human IgG Fc secondary Abs were then incubated with the samples for 45 min at room temperature. For all conditions, cells were washed 6 times with blocking buffer and 6 times with washing buffer (1.8 mM $CaCl_2$, 1 mM $MgCl_2$, 25 mM Tris [pH 7.5], and 140 mM NaCl). HRP enzyme activity was determined after the addition of a 1:1 mix of Western Lightning oxidizing and luminol reagents (PerkinElmer Life Sciences). Light emission was measured with an LB942 TriStar luminometer (Berthold Technologies). Signal obtained with parental HOS was subtracted for each plasma and was then normalized to the signal obtained with CR3022 mAb present in each plate. The seropositivity threshold was established using the following formula: mean of all SARS-CoV-2 negative plasma + (3 standard deviation of the mean of all SARS-CoV-2 negative plasma).

ADCC assay

The SARS-CoV-2 ADCC assay used was previously described (Anand et al., 2021; Beaudoin-Bussieres et al., 2020; Prevost et al., 2020). Briefly, parental CEM.NKr CCR5+ cells were mixed at a 1:1 ratio with CEM.NKr.Spike cells and were stained for viability (Aquavivid: Thermo Fisher Scientific) and a cellular dye (cell proliferation dye eFluor670; Thermo Fisher Scientific) to be used as target cells. Overnight rested PBMCs were stained with another cellular dye (cell proliferation dye eFluor450; Thermo Fisher Scientific), then used as effector cells. Stained target and effector cells were mixed at a ratio of 1:10 in 96-well V-bottom plates. Plasma from SARS-CoV-2 naive or PI individuals (1/500 dilution) or monoclonal antibody CR3022 (1 μg/mL) were added to the appropriate wells. The plates were subsequently centrifuged and incubated at 37°C, 5% CO_2 for 5 h before being fixed in a 2% PBS-formaldehyde solution. All samples were acquired on an LSRII cytometer (BD Biosciences) and data analysis was performed using FlowJo v10.7.1 (Tree Star).

Virus neutralization assay

The SARS-CoV-2 virus neutralization assay used was previously (Prevost et al., 2020). Briefly, 293T cells were transfected with the lentiviral vector pNL4.3 R-E- Luc plasmid (NIH AIDS Reagent Program) and a plasmid encoding for the full-length SARS-CoV-2 Spike D614G glycoprotein (Beaudoin-Bussieres et al., 2020; Prevost et al., 2020) at a ratio of 10:1. Two days post-transfection, cell supernatants were harvested and stored at −80°C until use. Pseudoviral particles were incubated with the indicated plasma dilutions (1/50; 1/250; 1/1,250; 1/6250; 1/31,250) for 1 h at 37°C and were then added to the 293T-ACE2 target cells followed by incubation for 48 h at 37°C. Then, cells were lysed and followed by one freeze-thaw cycle. An LB942 TriStar luminometer (Berthold Technologies) was used to measure the luciferase activity. The neutralization half-maximal inhibitory dilution (ID_{50}) represents the plasma dilution to inhibit 50% of the infection of 293T-ACE2 cells by SARS-CoV-2 pseudoviruses.

SARS-CoV-2-specific B cells characterization

To detect SARS-CoV-2-specific B cells, we conjugated recombinant RBD proteins with Alexa Fluor 488 or Alexa Fluor 594 (Thermo Fisher Scientific) according to the manufacturer's protocol. 2×10^6 frozen PBMC from SARS-CoV-2 naive and previously-infected donors were prepared in Falcon® 5mL-round bottom polystyrene tubes at a final concentration of 4×10^6 cells/mL in RPMI 1640 medium (GIBCO) supplemented with 10% of fetal bovine serum (Seradigm), Penicillin- Streptomycin (GIBCO) and HEPES (GIBCO). After a rest of 2 h at 37°C and 5% CO_2, cells were stained using Aquavivid viability marker (GIBCO) in DPBS (GIBCO) at 4°C for 20 min. The detection of SARS-CoV-2-antigen specific B cells was done by adding the RBD probes to the antibody cocktail listed in Table S1. Staining was performed at 4°C for 30 min and cells were fixed using 2% paraformaldehyde at 4°C for 15 min. Stained PBMC samples were acquired on Symphony cytometer (BD Biosciences) and analyzed using FlowJo v10.8.0 software.

Activation-induced marker (AIM) assay

The AIM assay (Morou et al., 2019; Niessl et al., 2020a, 2020b) was adapted for SARS-CoV-2 specific CD4 and CD8 T cells, as previously described (Tauzin et al., 2021b). PBMCs were thawed and rested for 3 h in 96-well flat-bottom plates in RPMI 1640 supplemented with HEPES, penicillin and streptomycin and 10% FBS. 1.7×10^6 PBMCs were stimulated with a S glycoprotein peptide pool (0.5 μg/mL per peptide, corresponding to the pool of 315 overlapping peptides (15-mers) spanning the complete amino acid sequence of the Spike glycoprotein (JPT) for 15 h at 37°C and 5% CO_2. CXCR3, CCR6, CXCR6 and CXCR5 antibodies were added in culture 15 min before stimulation. A DMSO-treated condition served as a negative control and *Staphylococcus enterotoxin B* SEB-treated condition (0.5 μg/mL) as positive control. Cells were stained for viability dye for 20 min at 4°C then surface markers (30 min, 4°C). Abs used are listed in the Table S2. Cells were fixed using 2% paraformaldehyde for 15 min at 4°C before acquisition on Symphony cytometer (BD Biosciences). Analyses were performed using FlowJo v10.8.0 software.

Intracellular cytokine staining (ICS)

The ICS assay adapted to study SARS-CoV-2-specific T cells was previously described (Tauzin et al., 2021b). PBMCs were thawed and rested for 2 h in RPMI 1640 medium supplemented with 10% FBS, Penicillin-Streptomycin (Thermo Fisher scientific, Waltham, MA) and HEPES (Thermo Fisher scientific, Waltham, MA). 1.7×10^6 PBMCs were stimulated with a S glycoprotein peptide pool (0.5 μg/mL per peptide from JPT, Berlin, Germany) corresponding to the pool of 315 overlapping peptides (15-mers) spanning the complete amino acid sequence of the S glycoprotein.

Cell stimulation was carried out for 6 h in the presence of mouse anti-human CD107a, Brefeldin A and monensin (BD Biosciences, San Jose, CA) at 37°C and 5% CO_2. DMSO-treated cells served as a negative control, and SEB as positive control. Cells were stained for Aquavivid viability marker (Thermo Fisher scientific, Waltham, MA) for 20 min at 4°C and surface markers (30 min, 4°C), followed by intracellular detection of cytokines using the IC Fixation/Permeabilization kit (Thermo Fisher scientific, Waltham, MA) according to the manufacturer's protocol before acquisition on a Symphony flow cytometer (BD Biosciences) and analysis using FlowJo v10.8.0 software. Abs used are listed in the Table S3.

QUANTIFICATION AND STATISTICAL ANALYSIS

Statistical analysis

Symbols represent biologically independent samples from SARS-CoV-2 naive individuals and SARS-CoV-2 PI individuals. Lines connect data from the same donor. Thick lines represent median values.

Linear mixed models fitting cell frequencies in terms of cohort, time point and their interaction were run using R and the package "nlme". Model diagnostics were performed, checking for heteroscedasticity and normality among residuals. Variance-covariance matrices were estimated using different weights for each time point, accounting for heteroscedasticity. All retained models used a square-root transform on the response variable, which helped in reducing the impact of outliers. Post-hoc contrasts across all pairwise comparisons of factor levels were obtained with the package "emmeans", correcting the p values by the method of Holm-Bonferroni where applicable. An important caveat of the square-root transform is that the reported contrast estimates and their confidence intervals remain on this scale, making their interpretation tricky. This was not deemed too great an obstacle, as qualitative statements on significant contrasts could be made based on p-values. Fifteen linear mixed models were retained, those being RBD B, AIM CD4, ICS CD4, AIM CD8, CXCR3, CXCR5, CXCR6, IFNg, IL-2, TNFa and CCR6 being compared between naive and PI co-

horts. There were also comparisons of PI donors receiving 1 dose vs 2 doses for RBD B, AIM CD4, ICS CD4 and AIM CD8. Models without satisfactory diagnostics were abandoned in favor of non-parametric methods. Differences in responses for the same patient before and after vaccination were performed using Wilcoxon matched pair tests. Differences in responses between naive and PI individuals were measured by Mann-Whitney tests. Wilcoxon and Mann-Whitney tests were generated using GraphPad Prism version 8.4.3 (GraphPad, San Diego, CA) (Rodda et al., 2022).

p values <0.05 were considered significant. p values are indicated for each comparison assessed. For descriptive correlations, Spearman's R correlation coefficient was applied. For graphical representation on a log scale (but not for statistical tests), null values were arbitrarily set at the minimal values for each assay. Complete statistical tests are centralized in the Table S4.

Software scripts and visualization

Graphics and pie charts were generated using GraphPad PRISM version 8.4.1 and ggplot2 (v3.3.3) in R (v4.1.0). Heat maps were generated in R (v4.1.0) using the pheatmap package (v1.0.12). Principal component analyses were performed with the prcomp function (R). Uniform manifold approximation and projection (UMAP) was performed using package M3C (v1.14.0) on gated FCS files loaded through the flowCore package (v2.4.0). Samples were down-sampled to a comparable number of events (300 cells for AIM, 100 cells for ICS). Scaling and logicle transformation of the flow cytometry data was applied using the FlowSOM (Quintelier et al., 2021) R package (v2.0.0). All samples from naive and PI at all time points were loaded. Clustering was achieved using Phenograph (v0.99.1) with the hyperparameter k (number of nearest-neighbors) set to 150). R codes scripted for this paper are provided as https://github.com/otastet/Nayrac_et_al. We obtained an initial 15 AIM+ and 11 cyto + clusters. After careful examination, five low-abundance AIM + clusters were merged based on proximity on the UMAP, phenotypic similarities and concomitant longitudinal trajectories. This resulted in a final 10 AIM + clusters. None of the 11 cyto + clusters were merged. For B and CD4+ T cell phenotyping, only participants with >5 RBD + B events across all depicted time points were analyzed.